Supplementary Information

Reversible ON-OFF switching of single-molecule-magnetism associated with single-crystal-to-single-crystal structural transformation of decanuclear dysprosium phosphonate

Haiquan Tian,[a] Jing-Bu Su,[b] Song-Song Bao,[a] Mohamedally Kurmoo,[c] Xin-Da Huang,[a] Yi-Quan Zhang,[b]* and Li-Min Zheng[a]*

[a]State Key Laboratory of Coordination Chemistry, Coordination Chemistry Institute, School of Chemistry and Chemical Engineering, Collaborative Innovation Center of Advanced Microstructures, Nanjing University, Nanjing 210023, P. R. China. E-mail: lmzheng@nju.edu.cn

[b]Jiangsu Key Laboratory for NSLSCS, School of Physical Science and Technology, Nanjing Normal University, Nanjing 210023, P. R. China. E-mail: zhangyiquan@njnu.edu.cn

[c]Universite de Strasbourg, Institut de Chimie, CNRS-UMR7177, 4 rue Blaise Pascal, Strasbourg Cedex 67007, France.

Computational details

Each of **I**, **I-UV** and **I-A-N_2** has five types of Dy^{III}, and **II-molecule A** and **II-molecule B** have three types of Dy^{III}, and thus five or three Dy^{III} fragments were calculated, respectively. Complete-active-space self-consistent field (CASSCF) calculations on individual lanthanide Dy^{III} fragments of the model structures (see Fig. S26 for the calculated model structures of **I**, **I-UV**, **I-A-N_2**, **II-molecule A** and **II-molecule B**) extracted from the compounds on the basis of single-crystal X-ray determined geometries have been carried out with MOLCAS 8.2 program package[S1] (see Fig. S32 for the complete structures of **I**, **I-UV**, **I-A-N_2**, **II-molecule A** and **II-molecule B**). Each dysprosium centre was calculated keeping the experimentally determined structure of the corresponding compound while replacing the other Dy^{III} ions by diamagnetic Lu^{III}. Besides, the influence of the neighbouring Dy^{III} ion was taken into account by the closed-shell La^{III} ab initio embedding model potentials (AIMP; La.ECP.deGraaf.0s.0s.0e-La-(LaMnO3.).[S2]

The basis sets for all atoms are atomic natural orbitals from the MOLCAS ANO-RCC library: ANO-RCC-VTZP for Dy^{III} ion; VTZ for close O and N; VDZ for distant atoms. The calculations employed the second order Douglas-Kroll-Hess Hamiltonian, where scalar relativistic contractions were taken into account in the basis set and the spin-orbit couplings were handled separately in the restricted active space state interaction (RASSI-SO) procedure. For the fragments of individual Dy^{III} ions, active electrons in 7 active spaces include all *f* electrons (CAS(9 in 7)) in the CASSCF calculation. To exclude all the doubts, we calculated all the roots in the active space. We have mixed the maximum number of spin-free state which was possible with our hardware (all from 21 sextets, 128 from 224 quadruplets, 130 from 490 doublets). And then, Single−Aniso[S3] program was used to obtain the *g* tensors, energy levels, magnetic axes, *et al.,* based on the above CASSCF/RASSI calculations.

References:

S1 (a) Aquilante, F.; De Vico, L.; Ferré, N.; Ghigo, G.; Malmqvist, P.-Å.; Neogrády, P.; Pedersen, T. B.; Pitonak, M.; Reiher, M.; Roos, B. O.; Serrano-Andrés, L.; Urban, M.; Veryazov, V.; Lindh, R. *J. Comput. Chem.*, **2010**, *31*, 224. (b) Veryazov, V.; Widmark, P. -O.; Serrano-Andres, L.; Lindh, R.; Roos, B. O. *Int. J. Quantum Chem.*, **2004**, *100*, 626. (c) Karlström, G.; Lindh, R.; Malmqvist, P. -Å.; Roos, B. O.; Ryde, U.; Veryazov, V.; Widmark, P. -O.; Cossi, M.; Schimmelpfennig, B.; Neogr´ady, P.; Seijo, L. *Comput.*

Mater. Sci., **2003**, *28*, 222.

S2 Seijo, L.; Barandiarán, Z. Computational Chemistry: Reviews of Current Trends; World Scientific, Inc.: Singapore, 1999; pp 455−152.

S3 (a) Chibotaru, L. F.; Ungur, L.; Soncini, A. *Angew. Chem. Int. Ed.*, **2008**, *47*, 4126. (b) Ungur, L.; Van den Heuvel, W.; Chibotaru, L. F. *New J. Chem.*, **2009**, *33*, 1224. (c) Chibotaru, L. F.; Ungur, L.; Aronica, C.; Elmoll, H.; Pilet, G.; Luneau, D. *J. Am. Chem. Soc.*, **2008**, *130*, 12445.

Table S1. Crystallographic and refinement data for **I-A-Ar-cool**.

formula	$C_{134}H_{128}Dy_{10}N_{32}O_{66}P_4$
M_r	4991.56
crystal size [mm^3]	0.2 × 0.3 × 0.4
T [K]	123(2)
crystal system	Monoclinic
space group	$P2_1/c$ #14
a [Å]	24.615(2)
b [Å]	14.566(1)
c [Å]	26.081(2)
α [°]	90
β[°]	112.968(2)
γ [°]	90
V [Å^3]	8609(1)
Z	2
ρ[g cm^{-3}]	1.926
2θ[deg]	2.0 –26.0
F(000)	4808
reflns collected	61489
unique reflns	16888
R_{int}	0.069
GOF	1.050
$R1$ [$I > 2\sigma(I)$][a]	0.0832
w$R2$ (all data)[b]	0.2017
$(\Delta\rho)_{max}$, $(\Delta\rho)_{min}$/[e Å^{-3}]	4.86, -3.64
CCDC	1819933

[a] $R_1 = \Sigma||F_o|-|F_c||/\Sigma|F_o|$. [b] $wR_2 = [\Sigma w(F_o^2-F_c^2)^2/\Sigma w(F_o^2)^2]^{1/2}$

Table S2. Selected bond lengths (Å) and angles (º) for compounds **I**, **I-UV**, **I-A-N$_2$** and **I-A-N$_2$-cool**.

	I	**I-UV**	**I-A-N$_2$**	**I-A-N$_2$-cool**
Dy1-O1	2.297(14)	2.272(19)	2.27(2)	2.27(2)
Dy1-O3	2.297(13)	2.305(17)	2.26(3)	2.30(2)
Dy1-O5	2.322(13)	2.276(16)	2.26(2)	2.320(18)
Dy1-O8	2.291(12)	2.307(13)	2.26(2)	2.301(17)
Dy1-O11	2.321(14)	2.30(2)	2.28(2)	2.34(2)
Dy1-O13	2.361(17)	-	2.34(3)	-
Dy1-O3W	-	2.36(2)	-	2.44(3)
Dy1-N1	2.528(15)	2.53(2)	2.56(3)	2.51(3)
Dy1-N7	2.550(18)	2.59(2)	2.60(3)	2.56(3)
Dy2-O1	2.497(14)	2.548(18)	2.61(2)	2.56(2)
Dy2-O2	2.500(13)	2.517(15)	2.57(2)	2.521(17)
Dy2-O6	2.217(13)	2.239(13)	2.25(2)	2.229(16)
Dy2-O8	2.439(12)	2.472(13)	2.48(2)	2.439(17)
Dy2-O9	2.623(13)	2.528(15)	2.57(2)	2.578(17)
Dy2-O14	2.376(14)	2.32(2)	2.26(3)	2.28(3)
Dy2-O1W	2.399(15)	2.43(2)	-	2.44(2)
Dy2-O16	-	-	2.34(3)	-
Dy2-N3	2.689(14)	2.64(2)	2.71(3)	2.63(3)
Dy2-N4	2.605(17)	2.58(2)	2.59(3)	2.64(3)
Dy3-O2	2.419(14)	2.400(15)	2.36(2)	2.41(2)
Dy3-O9	2.264(14)	2.282(14)	2.21(2)	2.288(16)
Dy3-O15	2.199(19)	2.49(2)	2.26(3)	2.51(3)
Dy3-O16	-	2.47(2)	-	2.52(3)
Dy3-O17	2.506(14)	2.449(16)	2.39(3)	2.47(2)
Dy3-O18	2.482(14)	2.472(14)	2.43(2)	2.474(16)
Dy3-O19	2.328(16)	2.340(16)	2.27(3)	2.334(18)
Dy3-O21	2.259(17)	2.334(16)	2.29(3)	2.33(2)
Dy3-N6	2.585(16)	2.595(15)	2.60(3)	2.59(2)
Dy4-O4	2.417(13)	2.426(13)	2.406(19)	2.410(15)
Dy4-O7	2.290(12)	2.287(14)	2.313(19)	2.280(17)
Dy4-O18	2.355(16)	2.369(17)	2.32(3)	2.345(18)
Dy4-O19	2.522(14)	2.482(14)	2.46(2)	2.499(15)
Dy4-O20	2.468(13)	2.462(15)	2.49(2)	2.468(16)
Dy4-O22	-	2.347(13)	2.38(3)	2.318(17)
Dy4-O23	2.386(17)	-	-	-
Dy4-O24	2.458(16)	2.427(16)	2.41(2)	2.466(16)
Dy4-O25	2.420(14)	-	2.40(2)	-
Dy4-O25A	-	2.440(14)	-	2.433(16)
Dy4-N12	2.594(14)	2.609(16)	2.61(2)	2.608(19)
Dy5-O3	2.459(13)	2.474(16)	2.52(3)	2.483(19)

Dy5-O4	2.550(14)	2.543(14)	2.58(2)	2.556(17)
Dy5-O5	2.408(13)	2.440(16)	2.445(19)	2.442(17)
Dy5-O7	2.565(12)	2.558(13)	2.565(18)	2.560(16)
Dy5-O10	2.242(13)	2.197(14)	2.19(2)	2.211(16)
Dy5-O12	2.321(15)	2.38(2)	2.31(2)	2.41(3)
Dy5-O26	2.416(16)	-	-	-
Dy5-O2W	-	2.349(18)	-	2.35(2)
Dy5-O1W	-	-	2.45(3)	-
Dy5-N9	2.650(17)	2.62(2)	2.67(4)	2.60(3)
Dy5-N10	2.601(17)	2.63(3)	2.64(3)	2.61(3)
Dy1-O1-Dy2	104.9(5)	109.5(7)	104.8(9)	107.5(9)
Dy1-O8-Dy2	107.0(5)	111.0(6)	109.3(9)	110.7(7)
Dy2-O2-Dy3	114.7(5)	113.8(6)	107.2(9)	114.5(6)
Dy2-O9-Dy3	115.7(5)	117.7(5)	112.3(9)	116.8(6)
Dy3-O18-Dy4	112.9(5)	110.5(6)	110.0(10)	111.0(7)
Dy3-O19-Dy4	112.4(6)	111.2(5)	110.8(9)	110.5(6)
Dy4-O4-Dy5	114.0(5)	113.2(5)	112.7(9)	113.6(6)
Dy4-O7-Dy5	118.2(5)	117.7(5)	116.4(7)	118.2(7)
Dy1-O3-Dy5	106.0(5)	106.4(6)	106.0(10)	106.1(7)
Dy1-O5-Dy5	106.9(5)	108.4(6)	108.4(8)	106.9(7)

Symmetry code: A: 1-x,1-y,1-z

Table S3. Selected bond lengths (Å) and angles (º) for compound **I-A-Ar-cool**.

Dy1-O1	2.311(14)	Dy3-O18	2.479(10)
Dy1-O3	2.296(13)	Dy3-O19	2.333(10)
Dy1-O5	2.300(11)	Dy3-O21	2.334(12)
Dy1-O8	2.301(10)	Dy3-N6	2.564(12)
Dy1-O11	2.323(15)	Dy4-O4	2.410(10)
Dy1-O3W	2.375(15)	Dy4-O7	2.292(10)
Dy1-N1	2.523(17)	Dy4-O18	2.362(11)
Dy1-N7	2.580(17)	Dy4-O19	2.505(10)
Dy2-O1	2.544(14)	Dy4-O20	2.470(10)
Dy2-O1W	2.430(15)	Dy4-O22	2.337(10)
Dy2-O2	2.518(10)	Dy4-O24	2.445(11)
Dy2-O6	2.237(11)	Dy4-O25A	2.425(10)
Dy2-O8	2.477(10)	Dy4-N12	2.584(12)
Dy2-O9	2.537(10)	Dy5-O3	2.480(13)
Dy2-O14	2.320(18)	Dy5-O4	2.570(10)
Dy2-N3	2.656(15)	Dy5-O5	2.441(10)
Dy2-N4	2.604(19)	Dy5-O7	2.536(10)
Dy3-O2	2.409(12)	Dy5-O10	2.220(11)
Dy3-O9	2.282(10)	Dy5-O12	2.386(14)
Dy3-O15	2.486(13)	Dy5-O2W	2.346(13)
Dy3-O16	2.466(13)	Dy5-N9	2.629(18)
Dy3-O17	2.459(12)	Dy5-N10	2.649(18)
Dy1-O1-Dy2	108.4(5)	Dy1-O3-Dy5	106.2(5)
Dy1-O8-Dy2	111.1(4)	Dy1-O5-Dy5	107.4(4)
Dy2-O2-Dy3	113.3(4)	Dy3-O18-Dy4	110.3(4)
Dy2-O9-Dy3	117.3(4)	Dy3-O19-Dy4	110.4(4)
Dy4-O7-Dy5	118.2(4)	Dy4-O4-Dy5	112.6(4)

Symmetry code: A: 1-x,1-y,1-z

Table S4. Selected bond lengths (Å) and angles (º) for compound **II**.

Dy1-O1	2.275(14)	Dy4-O24	2.408(14)
Dy1-O5	2.412(10)	Dy4-O27	2.369(17)
Dy1-O6	2.49(2)	Dy4-N9	2.576(15)
Dy1-O7	2.414(15)	Dy4-O16B	2.336(17)
Dy1-O8	2.311(9)	Dy4-O12	2.277(14)
Dy1-O25	2.32(3)	Dy4-O15	2.467(15)
Dy1-N1	2.581(15)	Dy4-O16	2.489(14)
Dy1-O8A	2.511(9)	Dy4-O17	2.403(17)
Dy1-O9A	2.453(10)	Dy4-O18	2.50(2)
Dy1-O26A	2.37(4)	Dy5-O24	2.565(14)
Dy2-O1	2.607(11)	Dy5-N12	2.565(15)
Dy2-O1W	2.371(11)	Dy5-O12	2.581(14)
Dy2-O2	2.445(10)	Dy5-O13	2.405(12)
Dy2-O4	2.513(11)	Dy5-O19	2.316(12)
Dy2-O5	2.530(12)	Dy5-O22	2.401(19)
Dy2-O10	2.361(14)	Dy5-O23	2.553(14)
Dy2-O3A	2.239(11)	Dy5-N13	2.670(17)
Dy2-N4	2.621(12)	Dy5-O14B	2.201(12)
Dy2-N5	2.663(13)	Dy6-O20B	2.353(15)
Dy3-O2	2.306(11)	Dy6-N15	2.55(2)
Dy3-O4	2.297(10)	Dy6-O13B	2.336(12)
Dy3-O11	2.328(12)	Dy6-O13	2.337(14)
Dy3-O2A	2.307(15)	Dy6-O20	2.352(14)
Dy3-O4A	2.297(10)	Dy6-O23	2.300(12)
Dy3-O11A	2.327(13)	Dy6-N15B	2.551(17)
Dy3-N7	2.536(14)	Dy6-O23B	2.301(13)
Dy3-N7A	2.535(17)		
Dy1-O8-Dy1A	112.3(4)	Dy4-O16-Dy4B	110.2(6)
Dy1-O1-Dy2	116.2(4)	Dy4-O12-Dy5	118.5(5)
Dy1-O5-Dy2	114.1(4)	Dy4-O24-Dy5	114.3(4)
Dy2-O2-Dy3	107.4(4)	Dy5-O13-Dy6	107.3(6)
Dy2-O4-Dy3	105.4(4)	Dy5-O23-Dy6	103.7(5)

Symmetry codes: A: 1/3+x-y, 2/3-y, 5/3-z; B: 2/3+y, -2/3+x, 4/3-z

Table S5. Dy^{III} geometry analysis of **I** by SHAPE 2.1 software.

Geometry (CN = 8)	**Dy1**	**Dy3**	**Geometry (CN = 9)**	**Dy2**	**Dy4**	**Dy5**
OP-8	30.240	30.716	EP-9	30.562	32.326	30.323
HPY-8	22.032	23.475	OPY-9	21.266	23.922	21.176
HBPY-8	15.205	12.747	HBPY-9	15.511	15.921	14.965
CU-8	10.013	10.321	JTC-9	11.393	14.413	9.946
SAPR-8	1.533	4.423	JCCU-9	6.153	9.644	6.815
TDD-8	1.397	3.263	CCU-9	4.827	7.966	5.594
JGBF-8	14.569	8.304	JCSAPR-9	9.953	2.839	7.929
JETBPY-8	26.119	25.099	CSAPR-9	8.908	1.727	7.006
JBTPR-8	3.050	3.109	JTCTPR-9	8.821	3.540	6.954
BTPR-8	2.133	3.296	TCTPR-9	9.990	2.784	8.056
JSD-8	4.657	2.674	JTDIC-9	11.855	12.345	11.316
TT-8	10.391	10.780	HH-9	2.716	8.916	3.284
ETBPY-8	20.861	21.990	MFF-9	6.982	1.759	5.408

Label	**Shape**	**Label**	**Shape**
OP-8	Octagon	EP-9	Enneagon (D_{9h})
HPY-8	Heptagonal pyramid (C_{7v})	OPY-9	Octagonal pyramid (C_{8v})
HBPY-8	Hexagonal bipyramid (D_{6h})	HBPY-9	Heptagonal bipyramid (D_{7h})
CU-8	Cube (O_h)	JTC-9	Johnson triangular cupola J3 (C_{3v})
SAPR-8	Square antiprism (D_{4d})	JCCU-9	Capped cube J8 (C_{4v})
TDD-8	Triangular dodecahedron (D_{2d})	CCU-9	Spherical-relaxed capped cube (C_{4v})
JGBF-8	Johnson gyrobifastigium J26 (D_{2d})	JCSAPR-9	Capped square antiprism J10 (C_{4v})
JETBPY-8	Johnson elongated triangular bipyramid J14 (D_{3h})	CSAPR-9	Spherical capped square antiprism (C_{4v})
JBTPR-8	Biaugmented trigonal prism J50 (C_{2v})	JTCTPR-9	Tricapped trigonal prism J51 (D_{3h})
BTPR-8	Biaugmented trigonal prism (C_{2v})	TCTPR-9	Spherical tricapped trigonal prism (D_{3h})
JSD-8	Snub diphenoid J84 (D_{2d})	JTDIC-9	Tridiminished icosahedron J63 (C_{3v})
TT-8	Triakis tetrahedron (T_d)	HH-9	Hula-hoop (C_{2v})
ETBPY-8	Elongated trigonal bipyramid (D_{3h})	MFF-9	Muffin (C_s)

Table S6. Dy^{III} geometry analysis of **I-UV** by SHAPE 2.1 software.

Geometry (CN = 8)	**Dy1**	**Geometry (CN = 9)**	**Dy3**	**Dy2**	**Dy4**	**Dy5**
OP-8	30.395	EP-9	34.477	30.765	33.003	30.946
HPY-8	22.420	OPY-9	23.614	21.270	23.315	20.885
HBPY-8	14.852	HBPY-9	15.710	14.488	16.441	14.867
CU-8	9.145	JTC-9	14.190	11.796	15.104	10.570
SAPR-8	1.702	JCCU-9	9.444	6.439	9.704	6.995
TDD-8	1.379	CCU-9	7.918	5.179	8.333	5.815
JGBF-8	14.931	JCSAPR-9	3.477	9.022	2.579	8.835
JETBPY-8	25.522	CSAPR-9	2.210	7.933	1.419	7.841
JBTPR-8	3.619	JTCTPR-9	3.103	8.047	3.285	7.837
BTPR-8	2.666	TCTPR-9	2.112	9.148	2.359	8.898
JSD-8	4.890	JTDIC-9	10.389	11.200	12.818	10.227
TT-8	9.432	HH-9	10.163	2.487	9.334	2.652
ETBPY-8	19.891	MFF-9	2.589	6.149	1.567	6.018

Table S7. Dy^{III} geometry analysis of **I-A-N_2** by SHAPE 2.1 software.

Geometry (CN = 8)	**Dy1**	**Dy3**	**Geometry (CN = 9)**	**Dy2**	**Dy4**	**Dy5**
OP-8	31.034	26.683	EP-9	29.539	34.414	29.904
HPY-8	21.907	22.601	OPY-9	19.569	23.428	21.449
HBPY-8	14.950	13.046	HBPY-9	14.833	17.337	15.178
CU-8	9.814	8.383	JTC-9	11.537	15.414	10.056
SAPR-8	1.552	2.669	JCCU-9	6.211	10.448	6.443
TDD-8	1.640	2.707	CCU-9	5.135	8.554	5.512
JGBF-8	14.358	10.448	JCSAPR-9	8.385	2.539	8.141
JETBPY-8	26.497	25.478	CSAPR-9	7.280	1.361	7.243
JBTPR-8	3.203	2.345	JTCTPR-9	7.268	3.924	6.998
BTPR-8	2.154	1.656	TCTPR-9	8.434	2.487	8.365
JSD-8	5.194	4.107	JTDIC-9	11.106	12.567	11.082
TT-8	10.051	9.047	HH-9	3.934	9.087	3.316
ETBPY-8	20.923	20.410	MFF-9	5.800	1.512	5.519

Table S8. Dy^{III} geometry analysis of **II** by SHAPE 2.1 software.

Geometry (CN = 8)	**Dy3**	**Dy6**	**Geometry (CN = 9)**	**Dy1**	**Dy2**	**Dy4**	**Dy5**
OP-8	29.505	29.745	EP-9	33.026	29.733	33.887	30.693
HPY-8	22.392	22.211	OPY-9	22.416	20.672	23.081	20.755
HBPY-8	15.835	15.914	HBPY-9	15.526	15.037	15.196	15.330
CU-8	9.735	10.294	JTC-9	13.959	11.074	14.474	10.640
SAPR-8	0.878	1.343	JCCU-9	8.783	6.056	9.532	6.615
TDD-8	1.719	1.550	CCU-9	7.325	4.759	8.165	5.469
JGBF-8	15.486	15.507	JCSAPR-9	3.751	10.031	3.186	8.957
JETBPY-8	26.272	25.862	CSAPR-9	2.647	9.182	2.111	7.882
JBTPR-8	3.286	3.386	JTCTPR-9	3.074	8.862	3.169	7.845
BTPR-8	2.366	2.438	TCTPR-9	2.492	10.186	2.376	9.049
JSD-8	5.142	4.834	JTDIC-9	11.428	10.963	11.126	11.528
TT-8	10.076	10.559	HH-9	9.304	2.436	9.675	2.979
ETBPY-8	20.968	20.539	MFF-9	2.887	7.351	2.505	6.166

Table S9. Relaxation fitting parameters from least-squares fitting of $\chi(\omega)$ data for compound **I-UV**.

T	χ_T	χ_s	α	ln(τ / s)
1.8	52.78	17.93	0.164	-8.330
2.0	48.81	15.12	0.158	-8.434
2.3	43.57	12.16	0.151	-8.506
2.6	38.18	8.56	0.148	-8.555
2.9	32.71	4.45	0.143	-8.589
3.2	27.49	0.49	0.141	-8.607
3.5	22.90	-1.95	0.135	-8.620
3.8	17.95	-5.21	0.134	-8.627
4.1	13.57	-8.24	0.133	-8.632
4.4	9.33	-12.79	0.131	-8.636
4.7	6.10	-15.61	0.130	-8.639
5.0	2.97	-18.94	0.129	-8.644
5.3	-0.47	-22.27	0.126	-8.648
5.6	-2.80	-25.17	0.125	-8.650
5.9	-5.53	-27.54	0.124	-8.651
6.2	-8.18	-30.87	0.123	-8.654
6.5	-10.19	-34.29	0.123	-8.664
6.8	-11.14	-36.65	0.122	-8.668
7.1	-13.12	-39.06	0.121	-8.680
7.4	-15.54	-41.45	0.120	-8.689
7.7	-17.45	-43.89	0.119	-8.703

Table S10. Magnetic relaxation parameters from least-squares fitting of $\chi(\omega)$ data for compound **I-A-Ar-cool**.

T	χ_T	χ_s	α	ln(τ / s)
1.8	52.78	17.93	0.164	-8.330
2.0	48.81	15.12	0.158	-8.434
2.3	43.57	12.16	0.151	-8.506
2.6	38.18	8.56	0.148	-8.555
2.9	32.71	4.45	0.143	-8.589
3.2	27.49	0.49	0.141	-8.607
3.5	22.90	-1.95	0.135	-8.620
3.8	17.95	-5.21	0.134	-8.627
4.1	13.57	-8.24	0.133	-8.632
4.4	9.33	-12.79	0.131	-8.636
4.7	6.10	-15.61	0.130	-8.639
5.0	2.97	-18.94	0.129	-8.644
5.3	-0.47	-22.27	0.126	-8.648
5.6	-2.80	-25.17	0.125	-8.650
5.9	-5.53	-27.54	0.124	-8.651
6.2	-8.18	-30.87	0.123	-8.654
6.5	-10.19	-34.29	0.123	-8.664
6.8	-11.14	-36.65	0.122	-8.668
7.1	-13.12	-39.06	0.121	-8.680
7.4	-15.54	-41.45	0.120	-8.689
7.7	-17.45	-43.89	0.119	-8.703

Table S11. Magnetic relaxation parameters from least-squares fitting of $\chi(\omega)$ data for compound **II**.

T	χ_T	χ_s	α	ln(τ / s)
1.8	42.86	3.86	0.247	-3.675
2.0	39.15	3.15	0.239	-3.694
3.0	31.75	2.84	0.207	-3.737
4.0	24.01	2.58	0.193	-4.074
5.0	18.81	2.28	0.185	-4.507
6.0	13.64	- 0.14	0.172	-4.979
7.0	9.37	-1.82	0.166	-5.453
8.0	6.36	-3.36	0.151	-5.929
9.0	3.76	- 4.76	0.143	-6.383
10.0	1.73	- 5.73	0.131	-6.821
11.0	0.09	- 6.59	0.122	-7.236
12.0	-1.48	- 7.51	0.115	-7.628
13.0	-3.28	- 8.71	0.106	-8.026
14.0	-4.91	-10.08	0.098	-8.436
15.0	-6.51	-11.48	0.084	-8.872
16.0	-7.79	-13.20	0.073	-9.305
17.0	-8.38	-15.61	0.063	-9.614
18.0	-8.68	-18.31	0.052	-9.969

Table S12. Calculated energy levels (cm^{-1}), ***g*** (g_x, g_y, g_z) tensors and m_J values of the lowest Kramers doublets (KDs) of the Dy^{III} fragments of **I**, **I-UV**, **I-A**, **II**-molecule **A** and **II**-molecule **B**.

KDs	**I**								
	Dy1			**Dy2**			**Dy3**		
	E/cm^{-1}	***g***	m_J	*E*/cm^{-1}	***g***	m_J	*E*/cm^{-1}	***g***	m_J
1	0.0	0.047 0.055 19.539	±15/2	0.0	0.178 0.328 19.206	±15/2	0.0	0.069 0.125 19.548	±15/2
2	70.7	0.748 1.079 15.327	±13/2	103.4	1.485 2.462 15.384	±13/2	75.2	0.550 0.833 16.465	±13/2
3	118.6	0.452 1.991 12.564	±11/2	171.2	9.269 6.597 3.772	±9/2	129.9	0.350 1.606 13.524	±11/2
4	174.0	8.111 7.272 0.011	±9/2	235.4	0.195 3.957 9.787	±3/2	187.4	2.622 4.326 10.357	±9/2
5	192.0	5.987 3.631 0.583	±1/2	262.1	0.524 3.009 14.504	±5/2	255.5	3.320 5.934 10.217	±7/2
6	222.3	9.458 6.977 1.705	±7/2	315.4	0.500 0.757 17.171	±7/2	339.8	1.403 2.481 15.199	±5/2
7	302.3	1.091 2.067 14.239	±3/2	369.3	0.206 0.317 15.477	±1/2	444.8	0.708 1.175 17.199	±3/2
8	372.9	0.450 1.247 17.622	±5/2	499.2	0.061 0.099 19.000	±11/2	482.4	0.392 1.682 17.956	±1/2

KDs	**I**					
	Dy4			**Dy5**		
	E/cm^{-1}	***g***	m_J	*E*/cm^{-1}	***g***	m_J
1	0.0	0.308 0.733 18.952	±15/2	0.0	0.520 3.386 15.278	±15/2
2	91.3	2.168 3.179 14.789	±13/2	15.1	0.751 2.796 14.265	±11/2
3	145.2	3.083 3.380 12.690	±9/2	157.9	2.381 4.219 13.506	±13/2
4	195.9	0.430	±5/2	201.0	1.693	±7/2

		3.941 12.491			5.001 10.151				
5	242.5	1.638 2.999 11.081	±1/2	254.1	0.817 3.991 11.275	±9/2			
6	319.0	0.094 0.148 18.667	±7/2	297.2	4.570 5.515 8.832	±5/2			
7	364.5	0.013 0.073 14.900	±3/2	370.5	1.121 1.634 14.637	±1/2			
8	473.6	0.047 0.062 18.514	±11/2	448.3	0.207 0.509 18.513	±3/2			
KDs	**I-UV**								
	Dy1			**Dy2**			**Dy3^{III}**		
	E/cm^{-1}	***g***	m_J	*E*/cm^{-1}	***g***	m_J	*E*/cm^{-1}	***g***	m_J
1	0.0	0.030 0.047 19.655	±15/2	0.0	0.196 0.373 19.402	±15/2	0.0	0.069 0.111 19.629	±15/2
2	71.7	0.677 0.974 15.535	±13/2	114.1	2.180 4.398 14.483	±11/2	77.2	0.911 1.412 16.151	±13/2
3	133.1	1.278 2.554 12.736	±7/2	180.3	8.412 5.842 1.994	±9/2	136.6	0.600 2.271 14.514	±11/2
4	195.0	0.621 4.251 10.329	±11/2	252.6	1.438 1.930 13.125	±3/2	197.1	2.625 4.470 11.487	±9/2
5	225.6	2.028 5.069 9.026	±3/2	293.5	0.337 1.208 17.112	±5/2	232.9	1.388 4.309 11.038	±5/2
6	248.7	0.439 2.432 16.164	±9/2	320.0	0.079 0.503 17.090	±1/2	307.8	1.927 2.717 14.887	±3/2
7	302.6	1.506 2.025 15.363	±5/2	384.7	0.134 0.256 15.540	±7/2	396.8	0.473 0.765 18.960	±1/2
8	401.2	0.220 0.481 18.806	±1/2	501.9	0.110 0.168 18.723	±13/2	531.2	0.039 0.098 19.507	±7/2
KDs	**I-UV**								
	Dy4			**Dy5**					
	E/cm^{-1}	***g***	m_J	*E*/cm^{-1}	***g***	m_J			

1	0.0	0.153 0.332 19.295	±15/2	0.0	0.165 0.272 19.083	±15/2			
2	120.8	1.165 1.808 15.521	±13/2	63.5	1.293 2.161 14.269	±13/2			
3	220.9	8.374 6.747 4.501	±11/2	107.3	0.988 2.759 11.845	±7/2			
4	304.0	1.797 2.462 11.188	±5/2	132.5	0.585 2.325 15.057	±11/2			
5	335.7	0.364 0.735 18.833	±1/2	165.9	8.485 6.788 2.097	±5/2			
6	402.9	0.054 0.073 17.487	±7/2	206.1	0.927 2.109 13.589	±9/2			
7	450.6	0.047 0.123 16.403	±3/2	281.5	1.000 1.676 14.529	±3/2			
8	605.4	0.013 0.037 19.060	±9/2	346.5	0.378 1.039 17.917	±1/2			
KDs	**I-A-N_2**								
	Dy1			**Dy2**			**Dy3**		
	E/cm^{-1}	***g***	m_J	*E*/cm^{-1}	***g***	m_J	*E*/cm^{-1}	***g***	m_J
1	0.0	0.193 0.259 19.567	±15/2	0.0	0.082 0.114 19.470	±15/2	0.0	0.125 0.297 19.125	±15/2
2	42.9	0.380 0.444 16.271	±13/2	126.8	1.298 2.516 15.083	±13/2	50.2	0.334 0.429 16.167	±13/2
3	104.0	2.539 4.124 9.381	±7/2	186.3	8.974 6.333 3.367	±9/2	117.9	1.296 2.297 13.649	±11/2
4	135.1	3.418 4.167 10.749	±3/2	261.0	1.316 2.870 9.607	±5/2	179.2	2.500 5.378 9.753	±9/2
5	162.7	0.968 3.269 13.738	±9/2	308.5	0.862 3.344 13.962	±3/2	263.1	2.833 5.731 10.888	±7/2
6	209.9	0.078 0.759	±11/2	342.9	1.186 3.602	±7/2	361.1	0.746 2.496	±3/2

		16.098			14.779			15.042	
7	262.9	0.538 0.704 15.996	±1/2	410.6	0.287 0.372 16.649	±1/2	455.9	1.503 3.465 13.507	±5/2
8	333.6	0.246 0.485 18.089	±5/2	581.7	0.028 0.054 19.336	±11/2	483.3	0.786 4.797 15.062	±1/2
KDs	**I-A-N_2**								
	Dy4			**Dy5**					
	E/cm^{-1}	***g***	m_J	*E*/cm^{-1}	***g***	m_J			
1	0.0	0.231 0.724 18.749	±15/2	0.0	0.016 0.018 19.741	±15/2			
2	81.3	2.449 4.457 12.673	±13/2	138.2	0.331 0.379 16.656	±13/2			
3	123.6	2.759 5.393 9.222	±9/2	199.6	1.929 2.473 13.192	±11/2			
4	194.3	0.641 4.669 9.207	±5/2	250.1	1.875 5.057 8.923	±9/2			
5	226.6	1.777 3.907 13.309	±1/2	303.7	3.488 4.142 8.449	±7/2			
6	307.5	0.059 0.177 18.722	±7/2	354.3	0.886 2.017 11.633	±5/2			
7	352.4	0.024 0.041 17.071	±3/2	466.4	0.216 0.405 17.065	±1/2			
8	472.1	0.004 0.009 18.901	±11/2	766.9	0.006 0.009 19.619	±3/2			
KDs	**II-molecule A**								
	Dy1			**Dy2**			**Dy3**		
	E/cm^{-1}	***g***	m_J	*E*/cm^{-1}	***g***	m_J	*E*/cm^{-1}	***g***	m_J
1	0.0	0.029 0.044 19.737	±15/2	0.0	0.179 0.365 19.238	±15/2	0.0	0.040 0.058 19.580	±15/2
2	106.2	0.455 0.833 16.216	±13/2	125.5	1.617 2.618 15.332	±13/2	71.9	0.752 1.338 15.913	±13/2
3	165.2	0.315	±11/2	195.5	3.431	±11/2	115.4	4.300	±9/2

		0.454 14.325			5.825 10.607			4.975 11.575	
4	229.0	3.824 3.905 10.754	±9/2	263.3	0.501 3.455 10.679	±7/2	160.6	0.140 4.073 8.601	±7/2
5	295.0	3.084 5.706 10.666	±7/2	312.2	1.883 2.848 15.117	±3/2	197.1	1.431 2.915 14.808	±11/2
6	390.8	1.031 2.457 15.275	±5/2	372.0	0.093 0.216 18.092	±1/2	253.6	1.351 2.170 11.455	±3/2
7	485.7	0.387 1.283 17.562	±1/2	416.4	0.144 0.503 14.961	±5/2	305.5	1.351 2.776 13.384	±5/2
8	532.3	0.365 1.418 18.233	±3/2	515.7	0.076 0.088 18.093	±9/2	379.2	0.320 0.530 18.359	±1/2
KDs	**II-molecule B**								
	Dy1			**Dy2**			**Dy3**		
	E/cm^{-1}	***g***	m_J	*E*/cm^{-1}	***g***	m_J	*E*/cm^{-1}	***g***	m_J
1	0.0	0.061 0.106 19.386	±15/2	0.0	0.348 0.767 18.964	±15/2	0.0	0.066 0.107 19.494	±15/2
2	58.0	0.378 0.428 16.300	±13/2	79.5	1.870 2.622 15.218	±11/2	78.1	1.138 1.839 15.569	±13/2
3	120.9	0.534 1.392 13.717	±11/2	130.9	3.144 5.207 11.465	±7/2	134.5	2.353 4.085 11.364	±11/2
4	168.8	3.349 4.615 9.557	±9/2	184.5	0.106 2.784 11.508	±1/2	206.6	2.446 5.286 9.027	±7/2
5	239.0	3.181 5.729 10.736	±7/2	219.6	0.587 2.878 14.337	±3/2	272.5	4.439 5.413 7.064	±5/2
6	336.3	0.600 2.511 14.929	±3/2	247.1	0.914 1.984 14.471	±5/2	319.2	2.776 3.916 9.666	±9/2
7	410.3	0.408 1.333 18.038	±1/2	314.0	0.172 0.304 15.405	±9/2	362.5	1.939 4.528 13.349	±3/2
8	482.9	0.169 0.506 18.972	±5/2	429.2	0.092 0.110 18.786	±13/2	465.6	0.135 0.222 19.117	±1/2

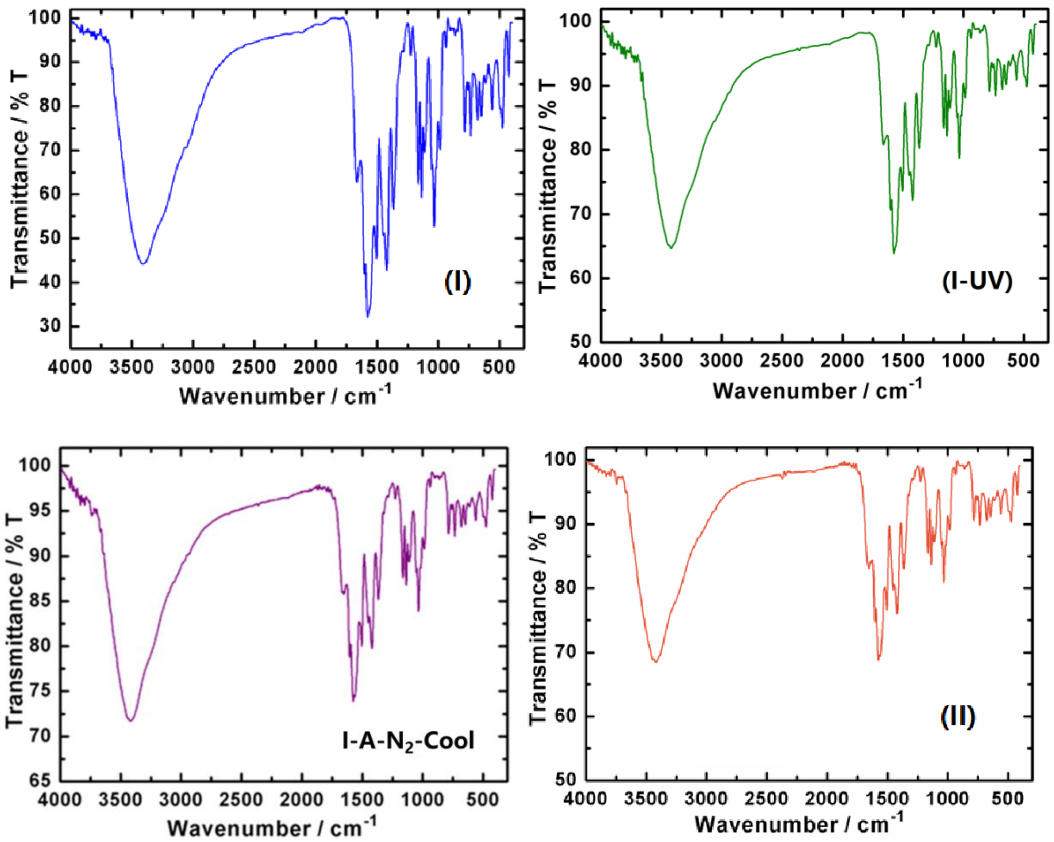

Figure S1. Infrared spectra of compounds **I**, **I-UV**, **I-A-N_2-cool** and **II**.

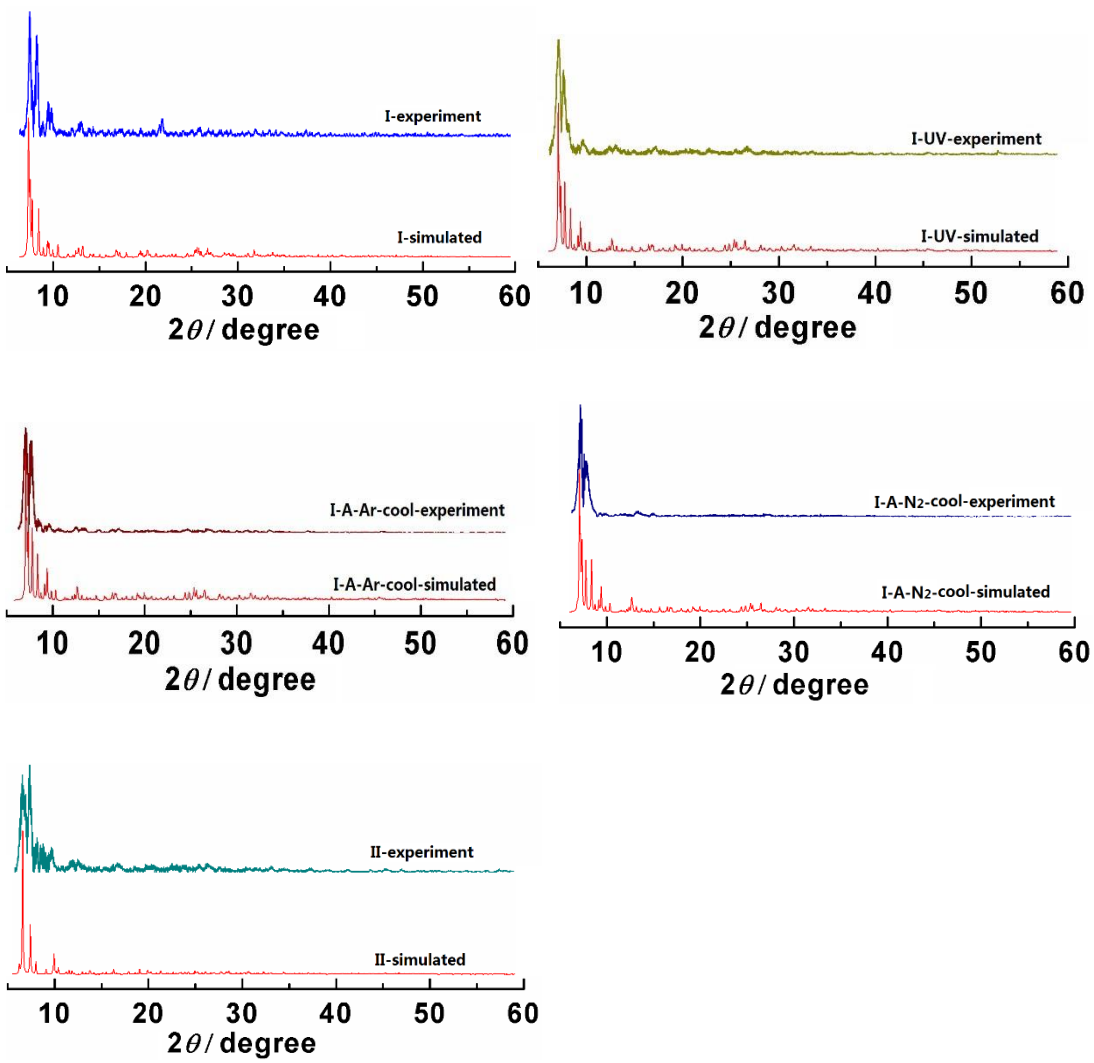

Figure S2. Powder XRD patterns for compounds **I**, **I-UV**, **I-A-N_2-cool**, **I-A-Ar-cool** and **II**.

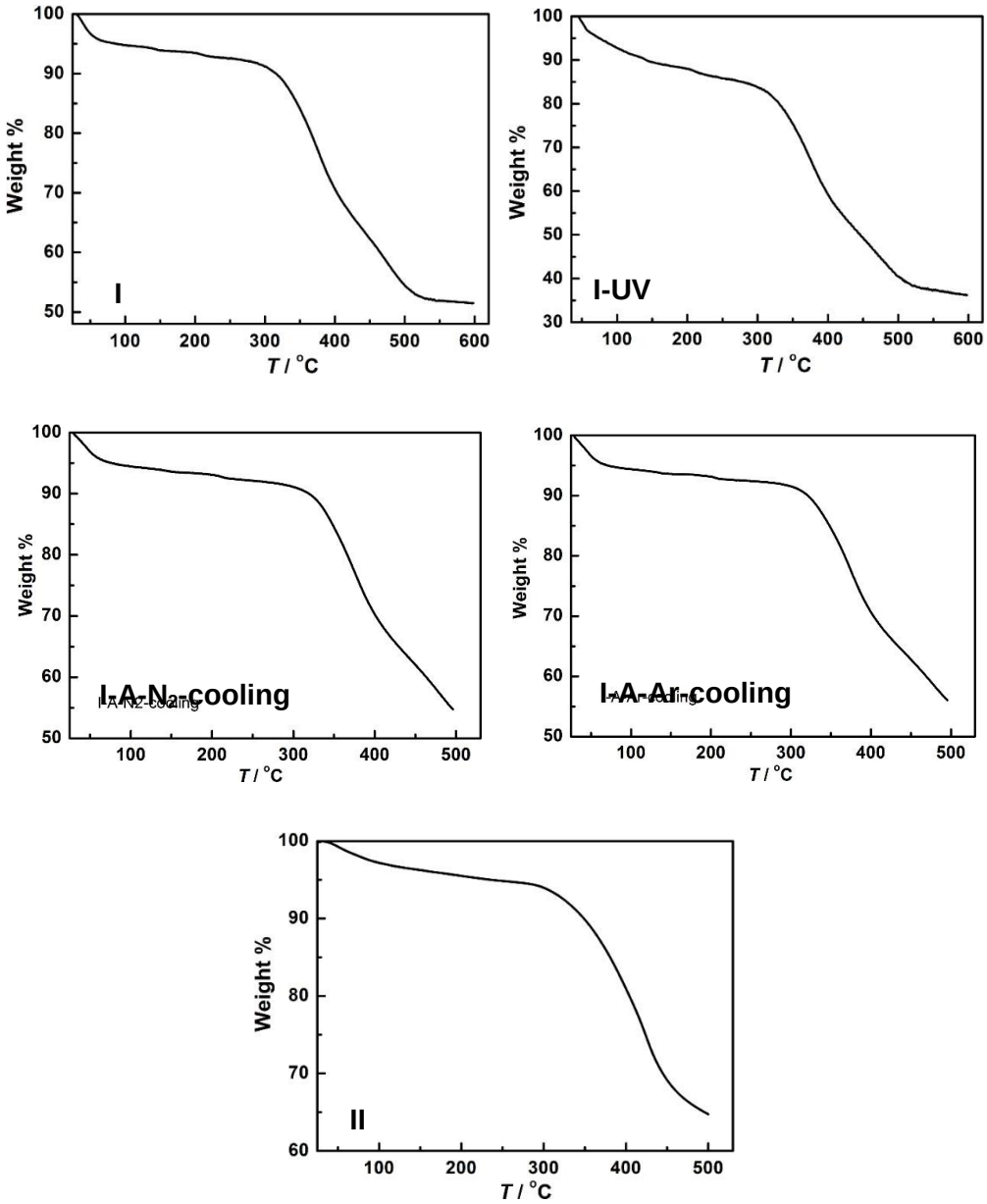

Figure S3. Thermal analyses of compounds **I**, **I-UV**, **I-A-N_2-cooling**, **I-A-Ar-cooling** and **II**. For **I**, the weight loss at 120 °C is 5.5%, corresponding to the removal of two coordination water and methanol and six lattice water molecules (calcd. 5.5%). For **I-UV**, the weight loss at 120 °C is 10.5%, corresponding to the removal of six coordination and 24 lattice water molecules (calcd. 10.0%). For **I-A-N_2-cooling** and **I-A-Ar-cooling**, the weight losses at 120 °C are 5.2% and 5.9%, respectively, corresponding to the removal of six coordination and nine (for the former) or eleven (for the latter) lattice water molecules (calcd. 5.4% and 6.1%, respectively). For **II**, the weight loss at 200 °C is 4.5%, corresponding to the removal of two lattice chloroform molecules (calcd. 4.7%).

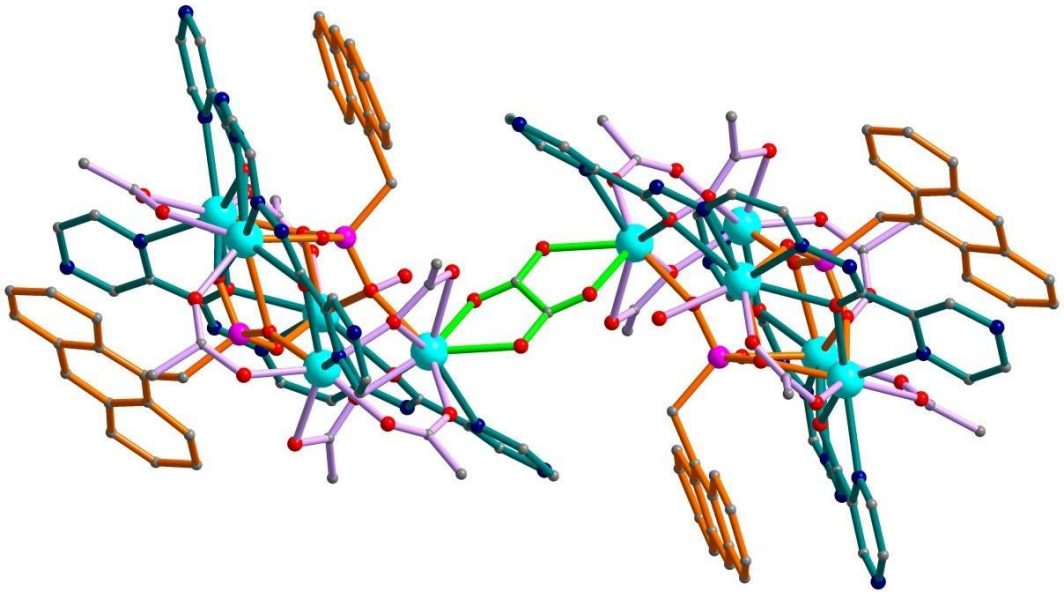

Figure S4. Side-view of compound **I**. Turquiose Dy, Red O, Blue N, purple P, grey C.

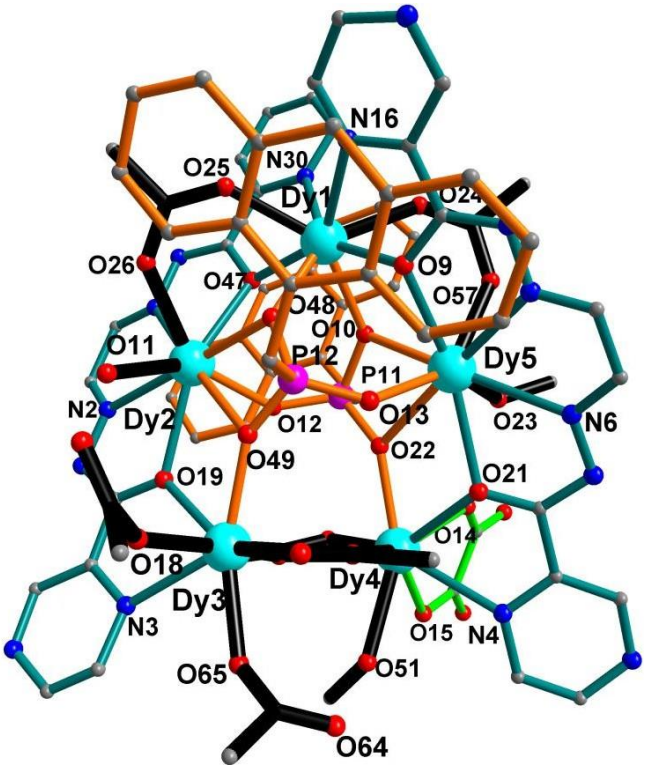

Figure S5. Partially labelled structure of the asymmetric unit of **I**. Turquiose Dy, Red O, Blue N, purple P, grey C.

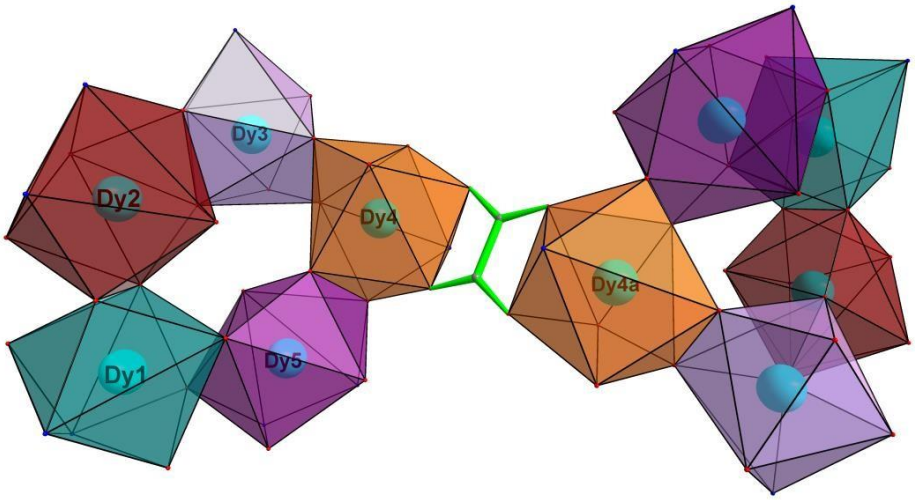

Figure S6. Coordination polyhedra observed for the metal centre in **I**. Turquiose Dy, Red O, Blue N, grey C.

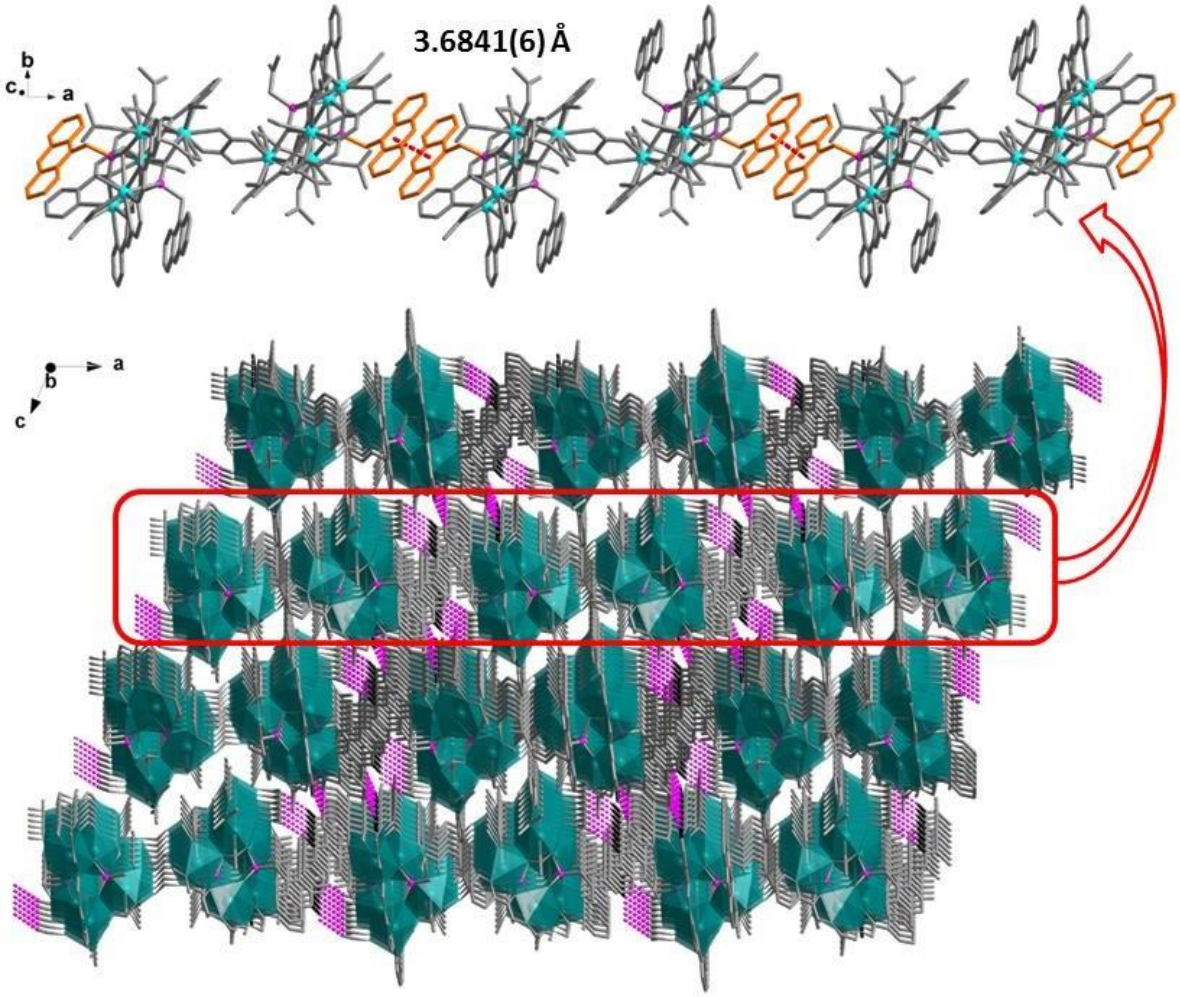

Figure S7. Top: supramolecular chain structure based on the π···π stacking interactions anthracene moieties. Bottom: 3D hydrogen-bonded supramolecular structure of compound **I**. Turquiose Dy, Red O, Blue N, C Gray, H Black.

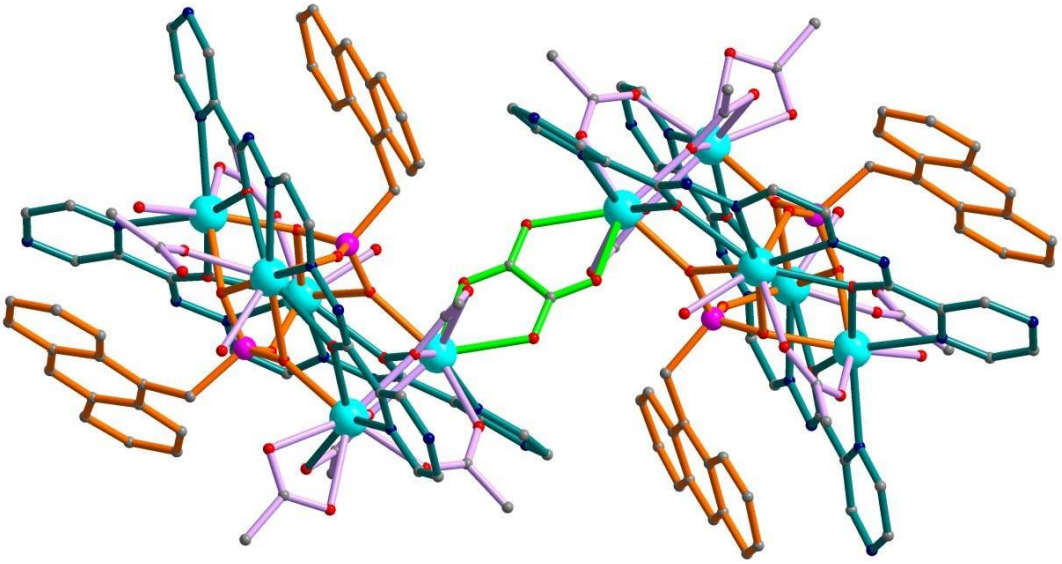

Figure S8. Side-view of compound **I-UV**. Turquiose Dy, Red O, Blue N, purple P, grey C.

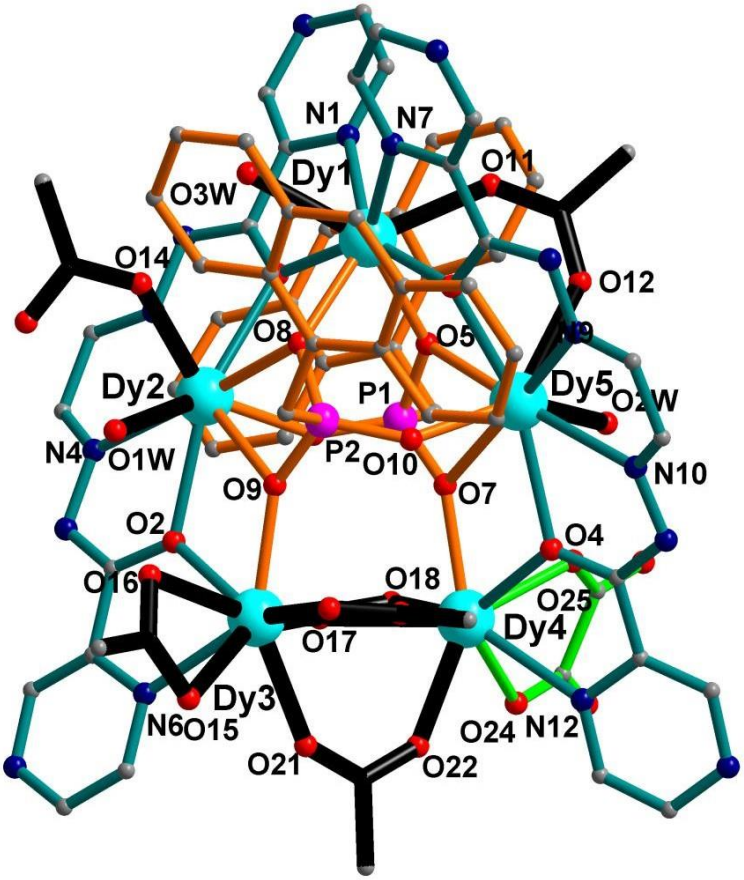

Figure S9. Partially labelled structure of the asymmetric unit of **I-UV**. Turquiose Dy, Red O, Blue N, purple P, grey C.

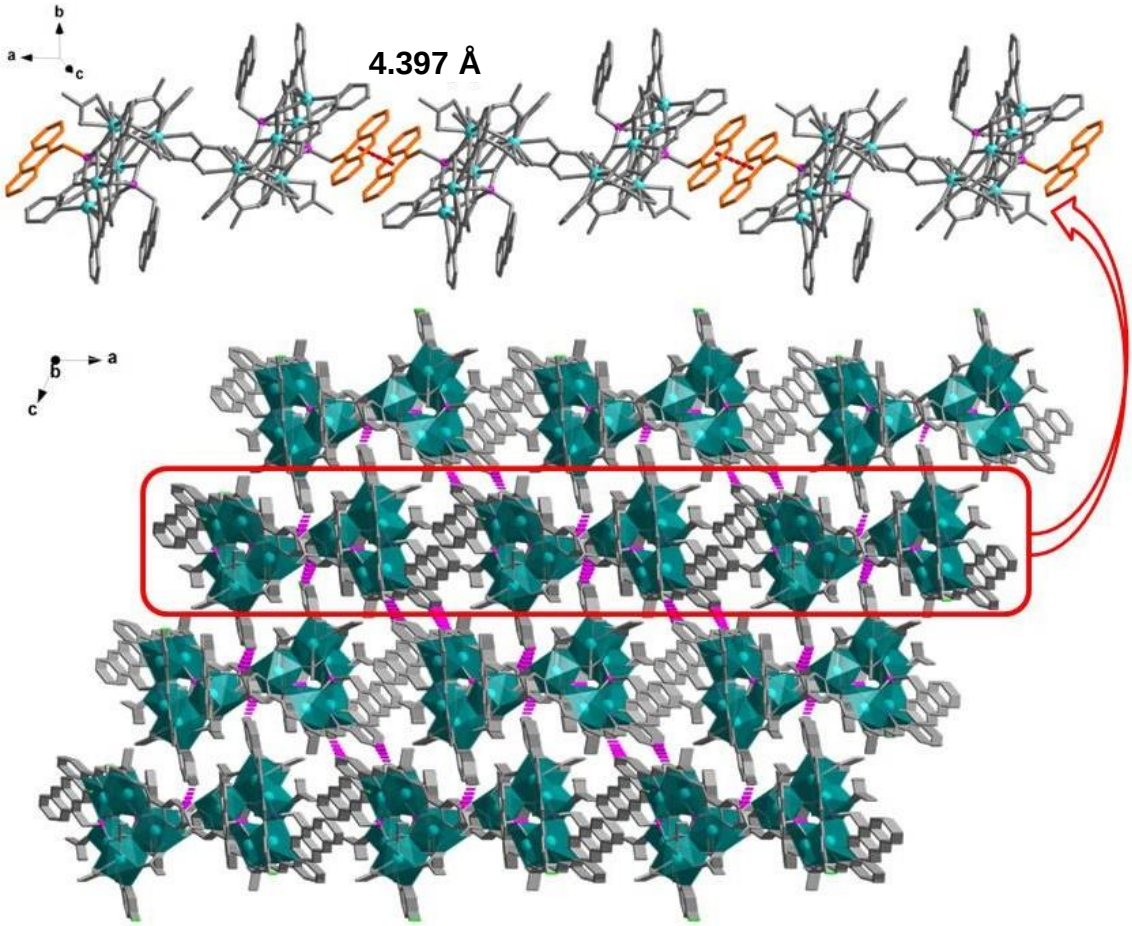

Figure S10. Top: supramolecular chain structure based on the π···π stacking interactions anthracene moieties. Bottom: 3D hydrogen-bonded supramolecular structure of compound **I-UV**. Turquiose Dy, Red O, Blue N, C Gray, H Bright green.

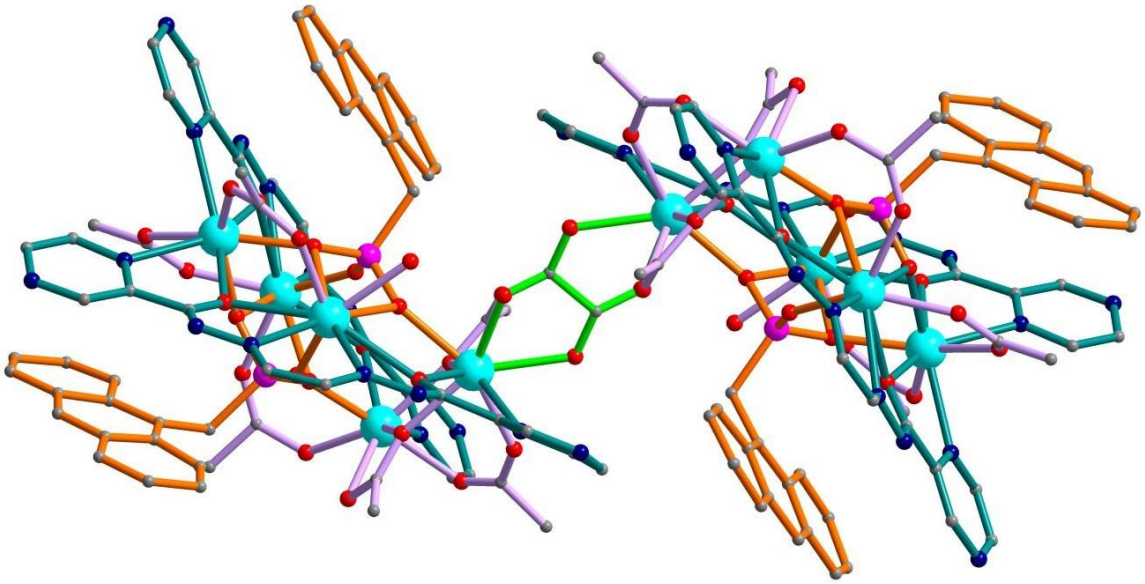

Figure S11. Side-view of compound **I-A-N$_2$**. Turquiose Dy, Red O, Blue N, purple P, grey C.

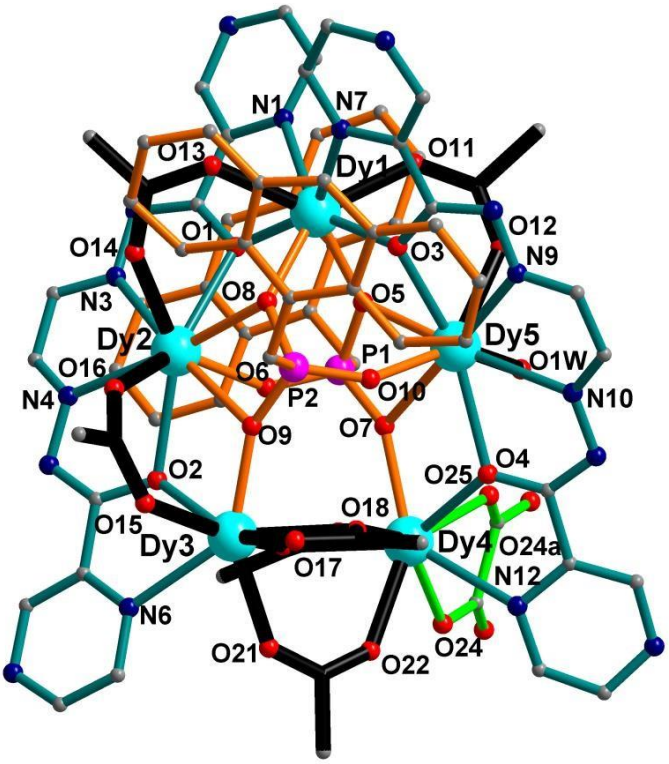

Figure S12. Partially labelled structure of the asymmetric unit of **I-A-N$_2$**. Turquiose Dy, Red O, Blue N, purple P, grey C.

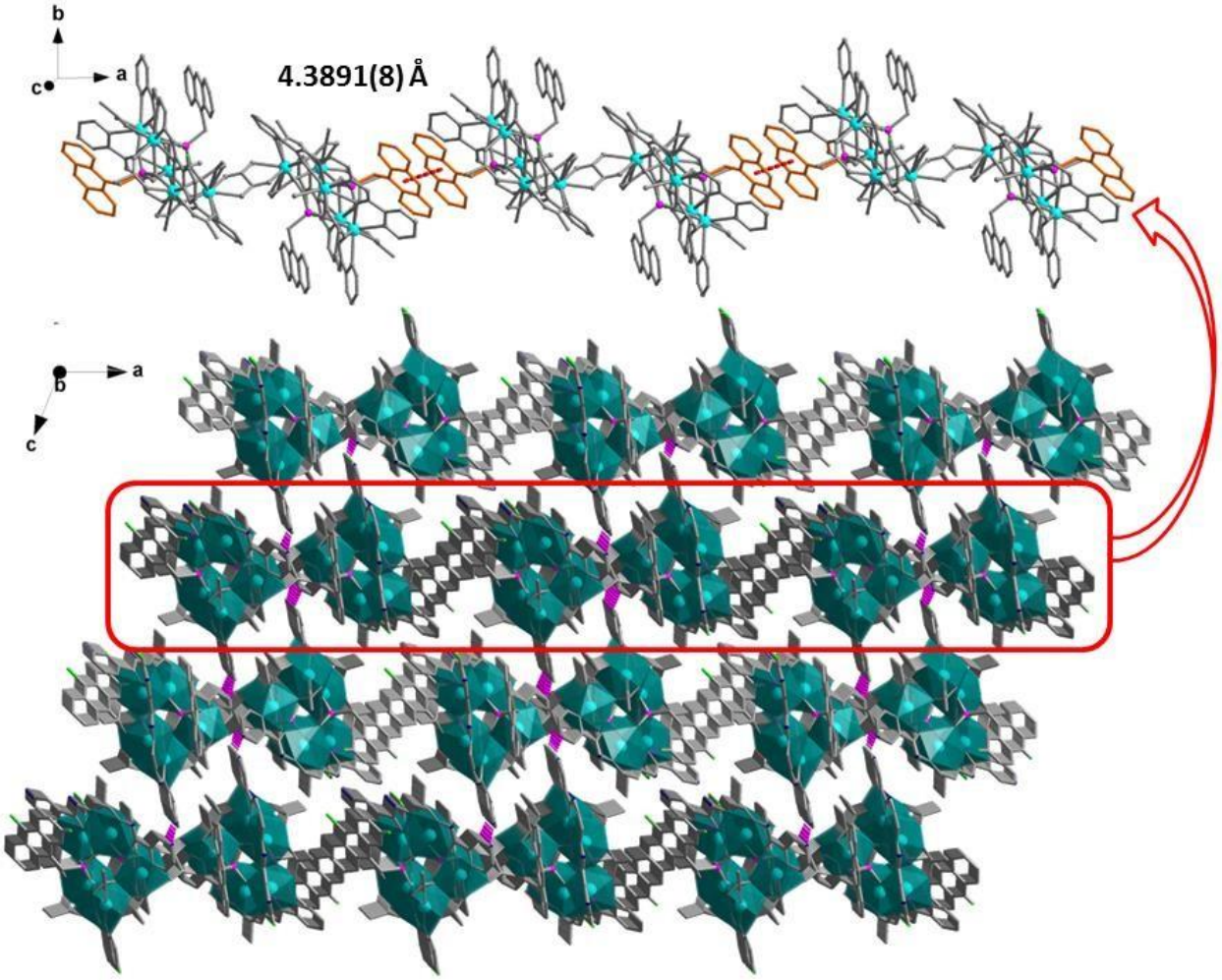

Figure S13. Top: supramolecular chain structure based on the π···π stacking interactions anthracene moieties. Bottom: 3D hydrogen-bonded supramolecular structure of compound **I-A-N$_2$**. Turquiose Dy, Red O, Blue N, C Gray, H Bright green.

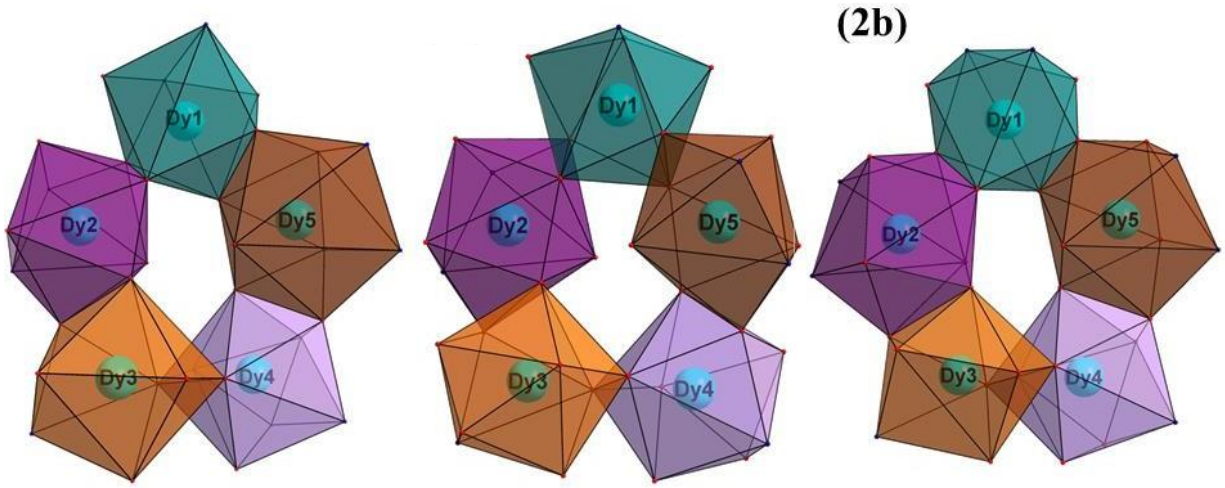

Figure S14. Coordination polyhedra observed for the metal centres in the asymmetric units of compounds **I** (left), **I-UV** (middle) and **I-A-N$_2$** (right).

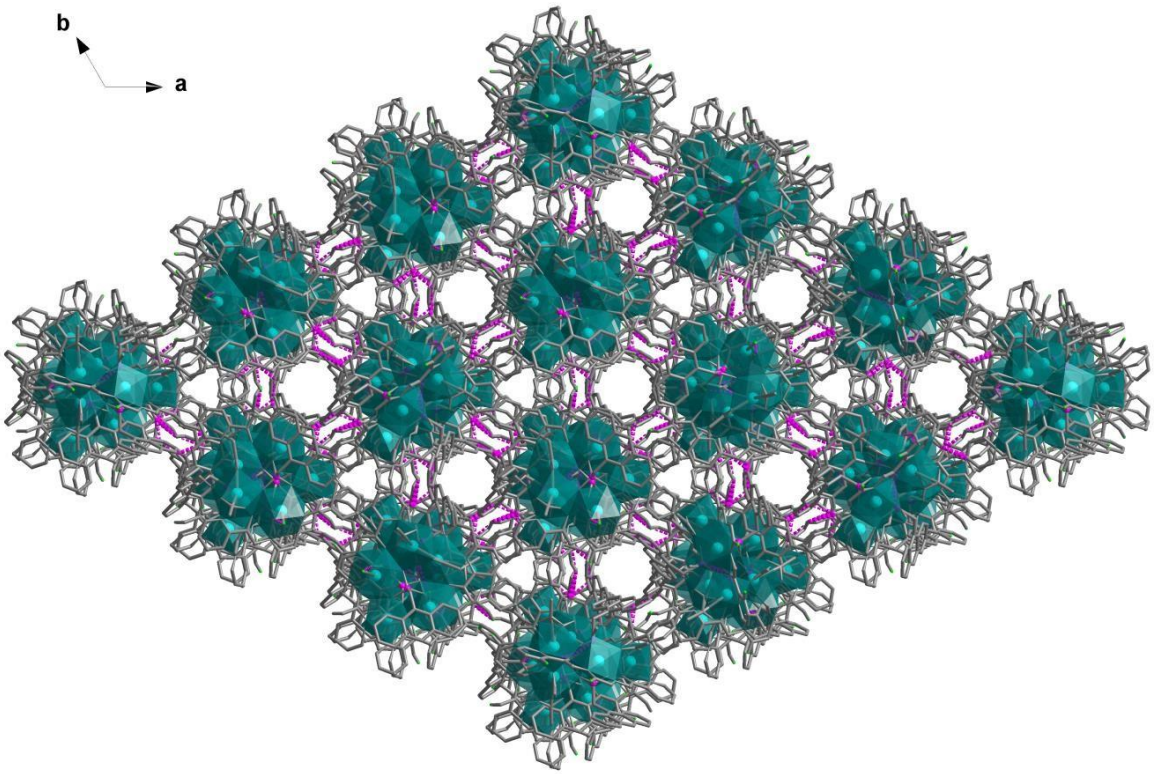

Figure S15. Packing arrangement of the molecules along a axis in **II**. Turquiose Dy, Red O, Blue N, C Gray, H Bright green.

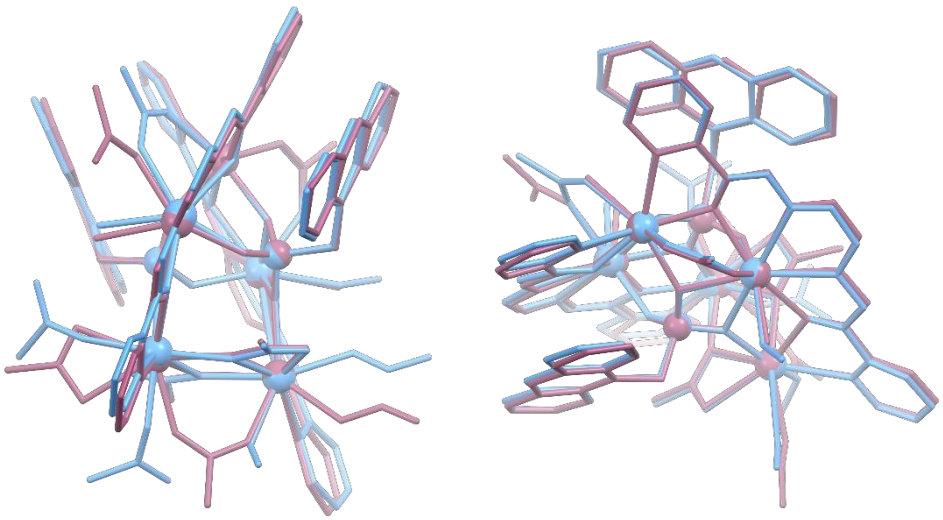

Figure S16. Overlay of the asymmetric molecules of **I** (blue) and **I-UV** (purple red).

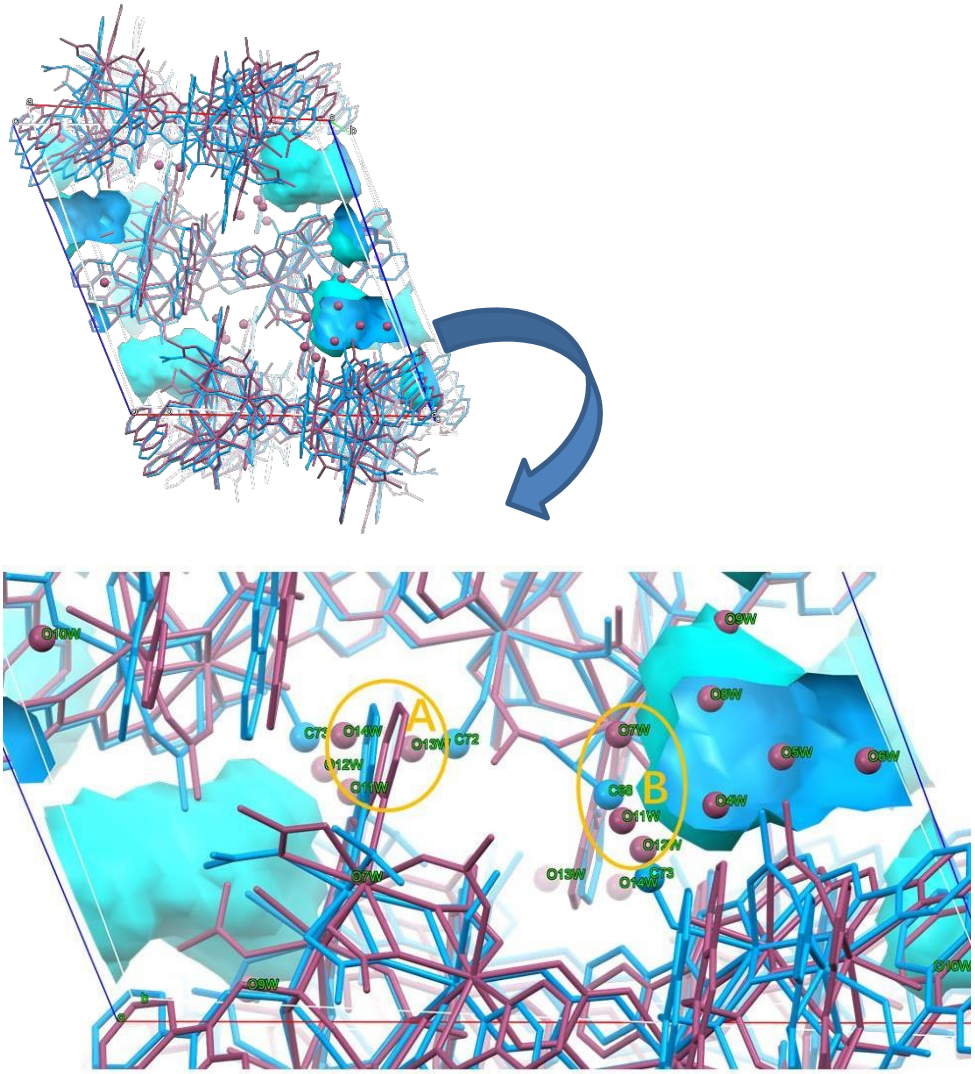

Figure S17. Overlay of the unit cells of **I** (blue) and **I-UV** (purple red). All of possible solvents in **I** were squeezed and empty space (voids) in unit cell is shown in blue (outside, light blue; inside, sky blue).

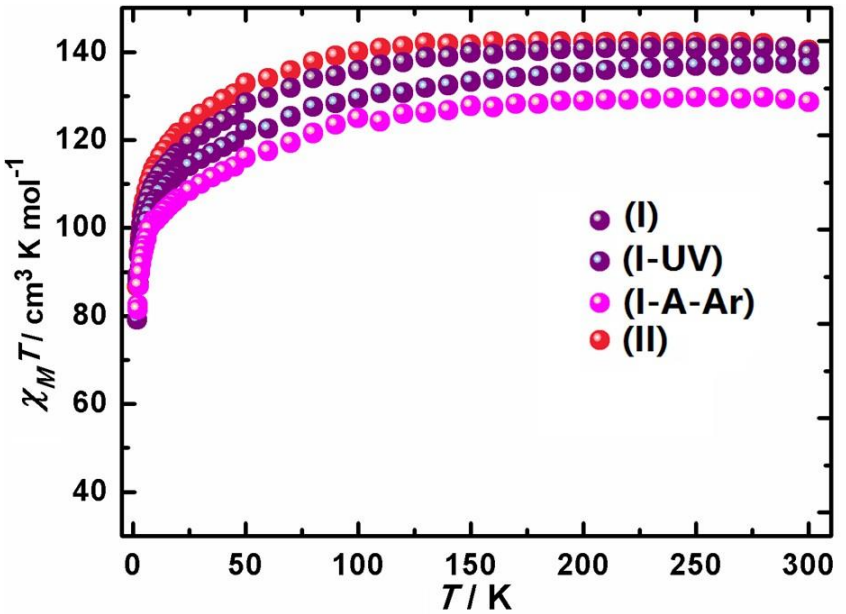

Figure S18. Temperature dependence of the $\chi_M T$ product at 1 kOe for **I**, **I-UV, I-A-Ar** and **II** per Dy_{10}.

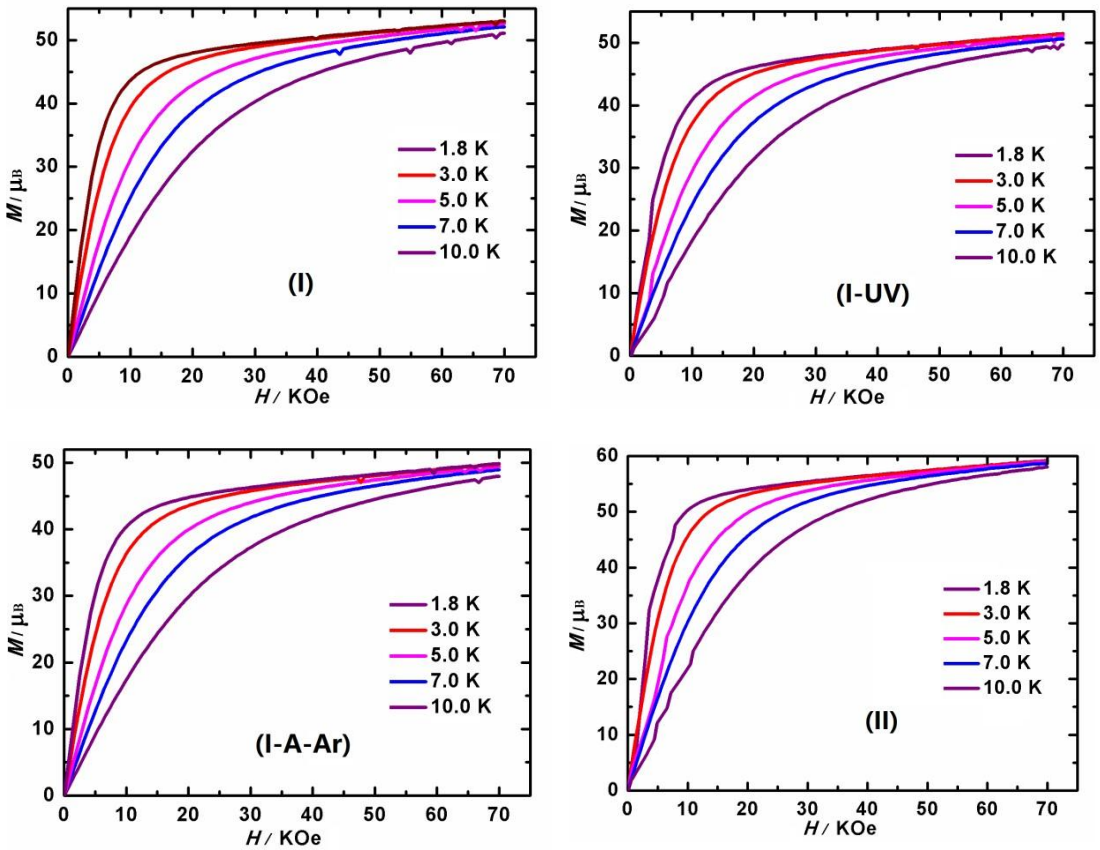

Figure S19. Isothermal magnetization at different temperatures.

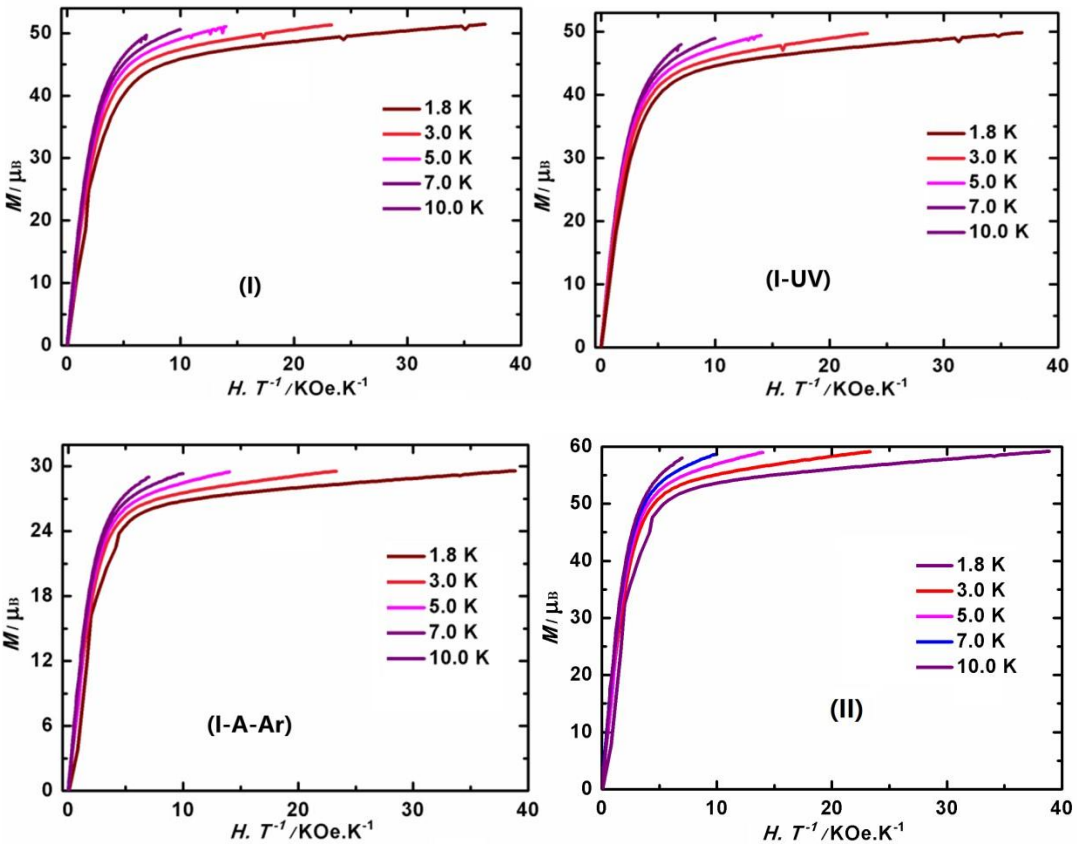

Figure S20. *M vs. H/T* plot at different temperatures below 10.0 K for **I**, **I-UV**, **I-A-Ar** and **II**.

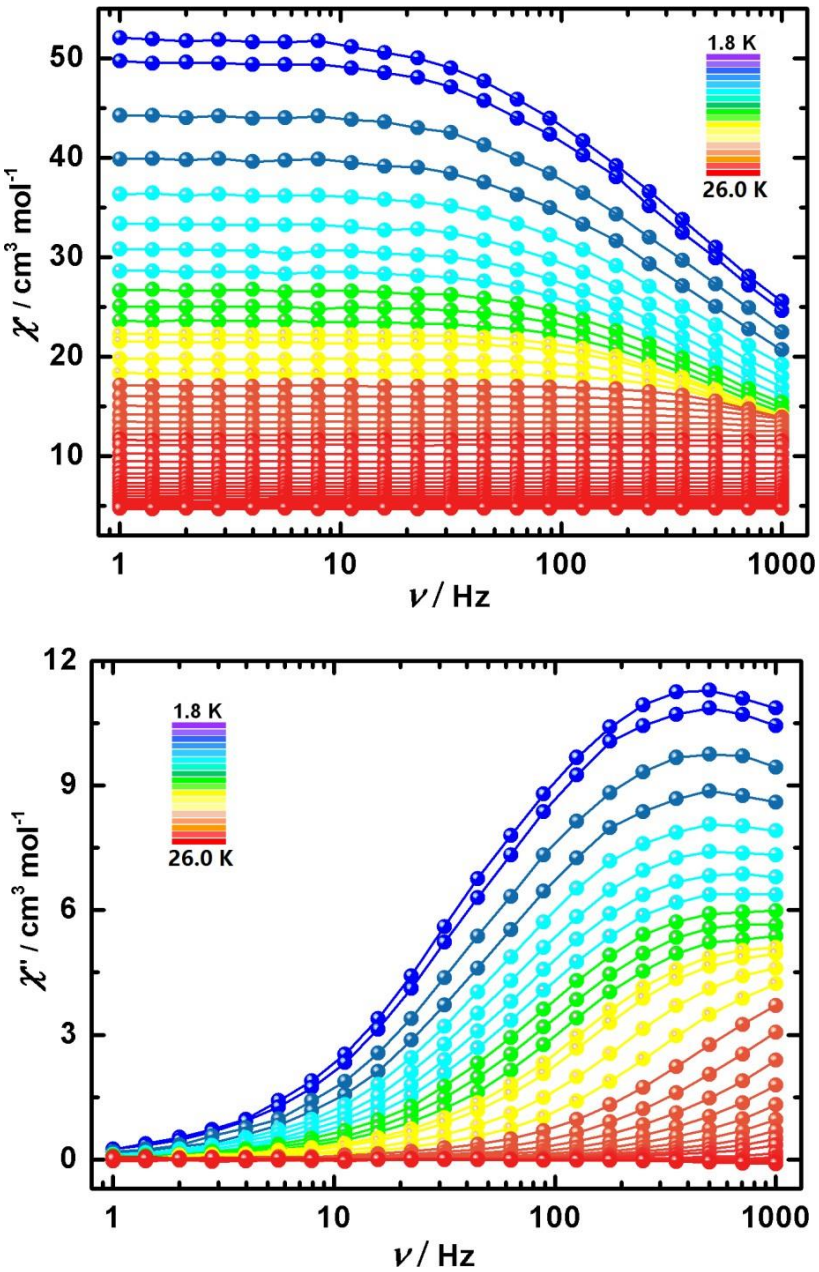

Figure S21. Frequency dependence of the χ' and χ'' of the *ac* susceptibilities under zero-dc field for compound **I-UV**.

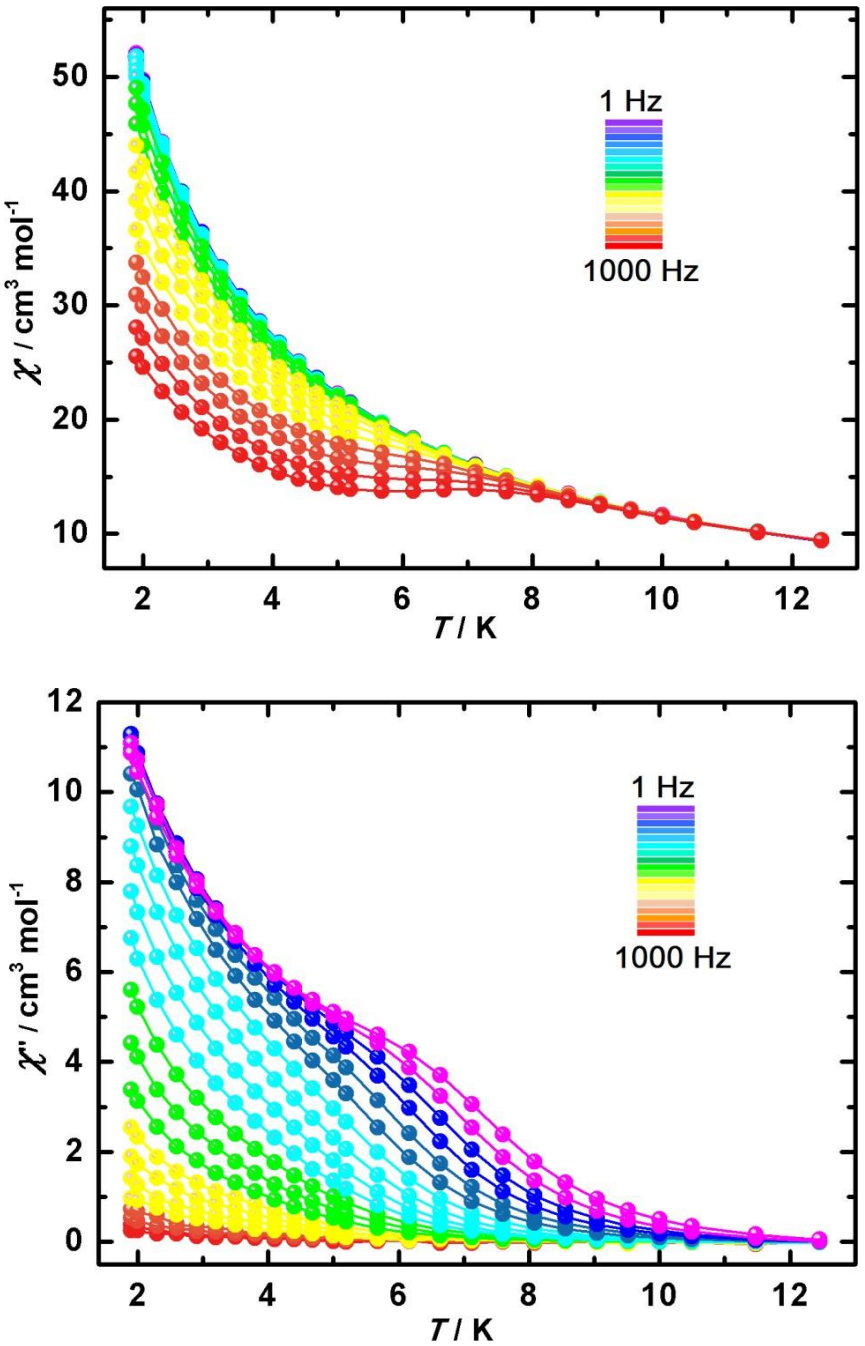

Figure S22. Temperature dependence of the χ' and χ'' of the *ac* susceptibilities under zero-dc field for compound **I-UV**.

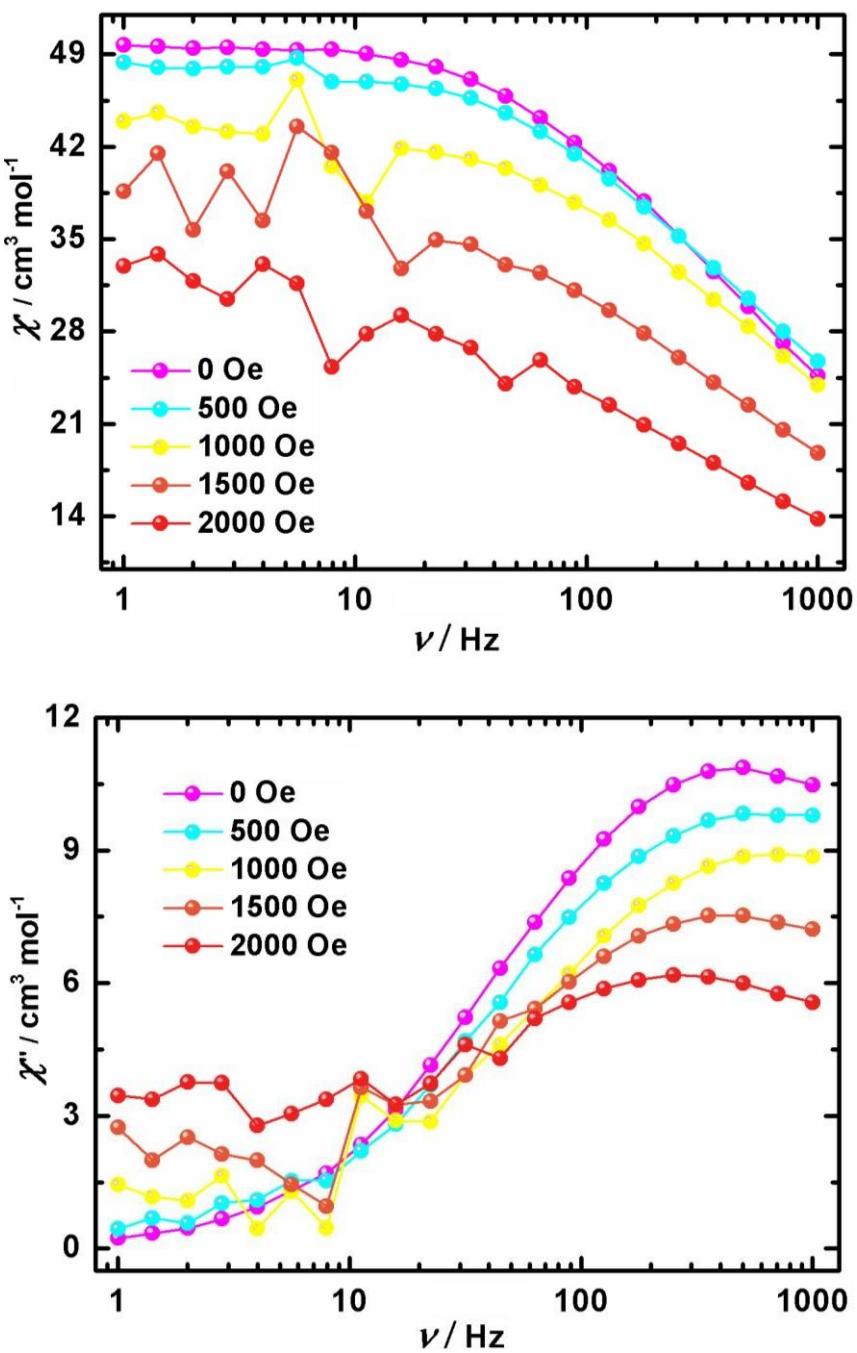

Figure S23. The in-phase (χ') and out-of-phase (χ'') ac susceptibilities as a function of the dc applied field measured at 2.0 K for compound **I-UV**.

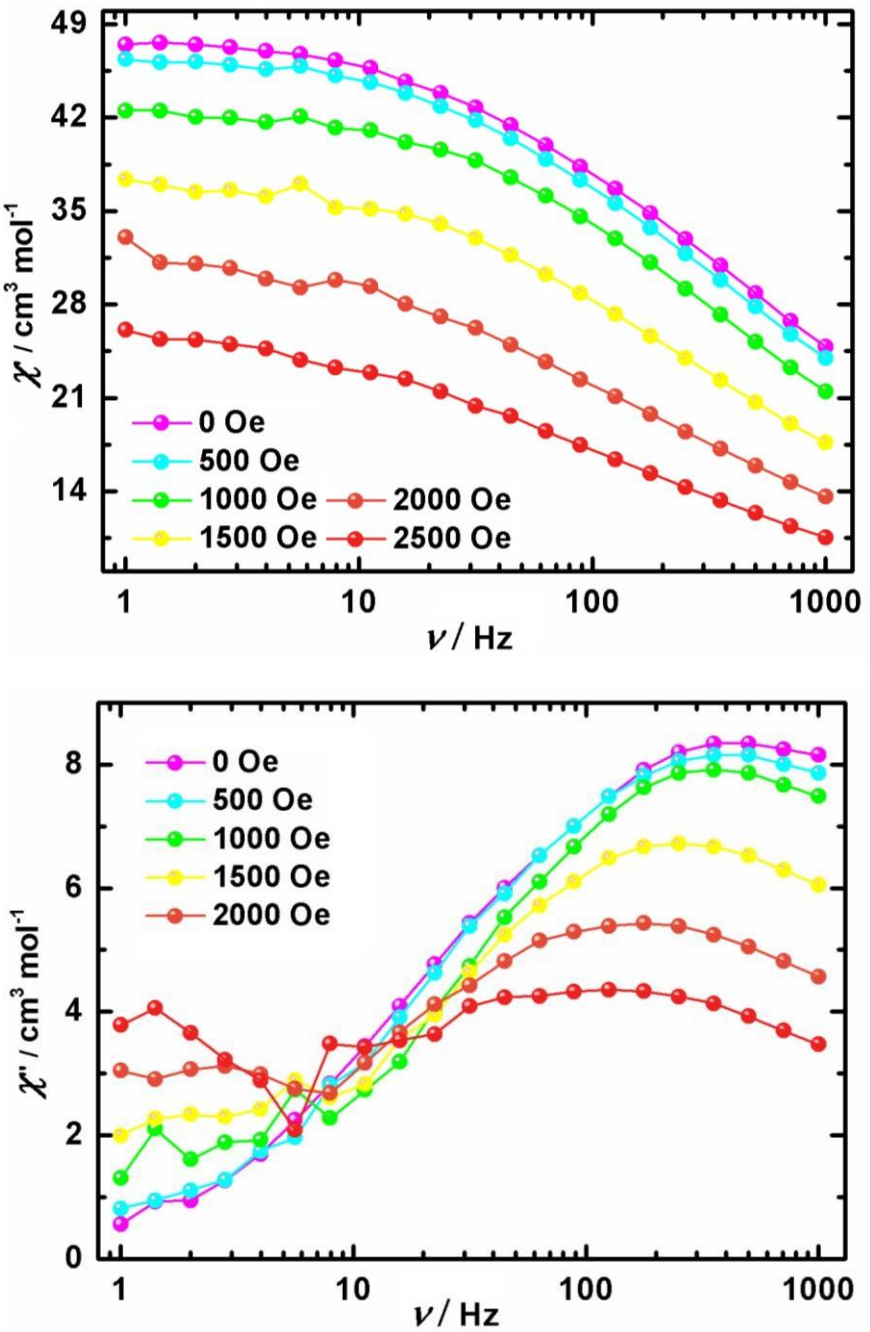

Figure S24. The in-phase (χ') and out-of-phase (χ'') ac susceptibilities as a function of the dc applied field measured at 2.0 K for compound **I-A-Ar-cool**.

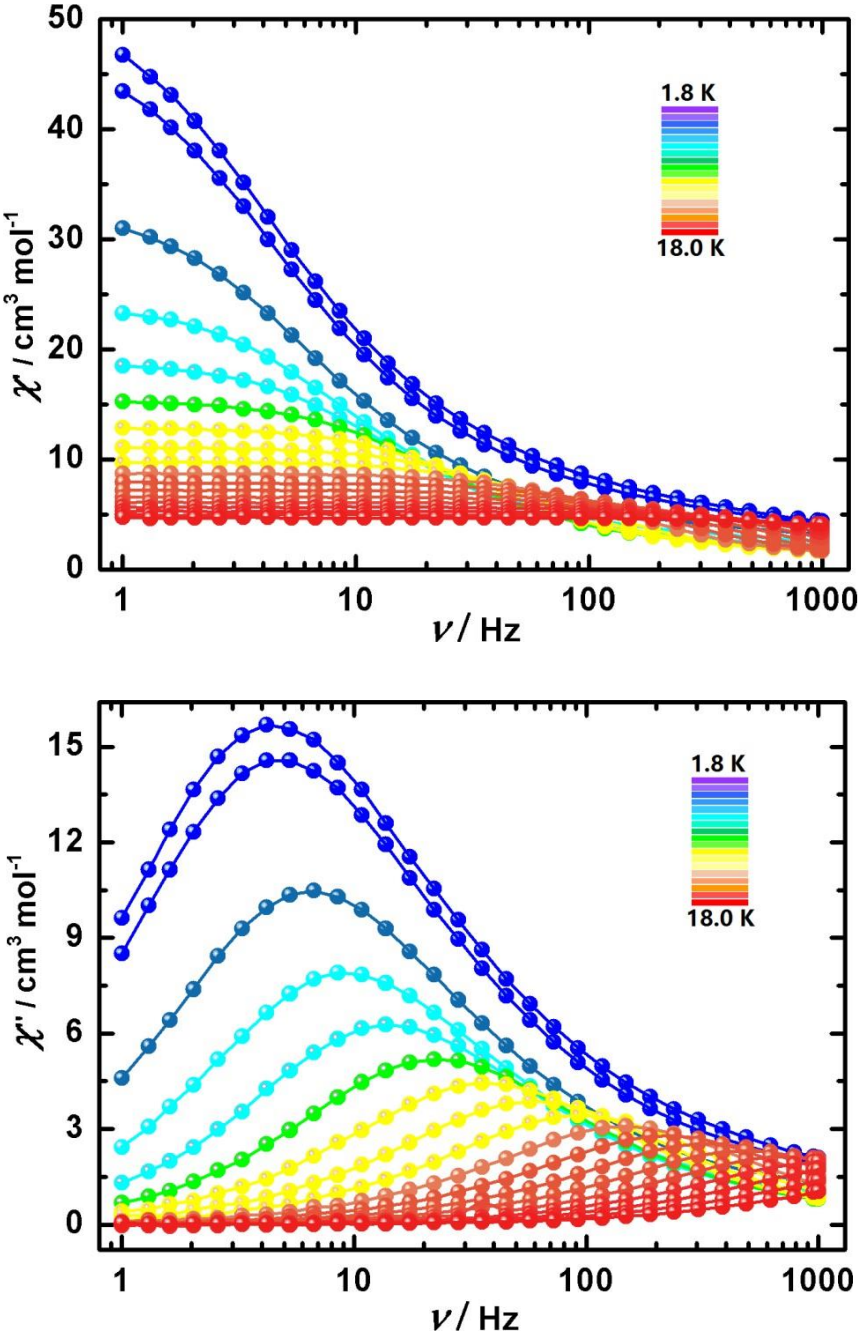

Figure S25. Frequency dependence of the χ' and χ'' of the *ac* susceptibilities under zero-dc field for compound **II**.

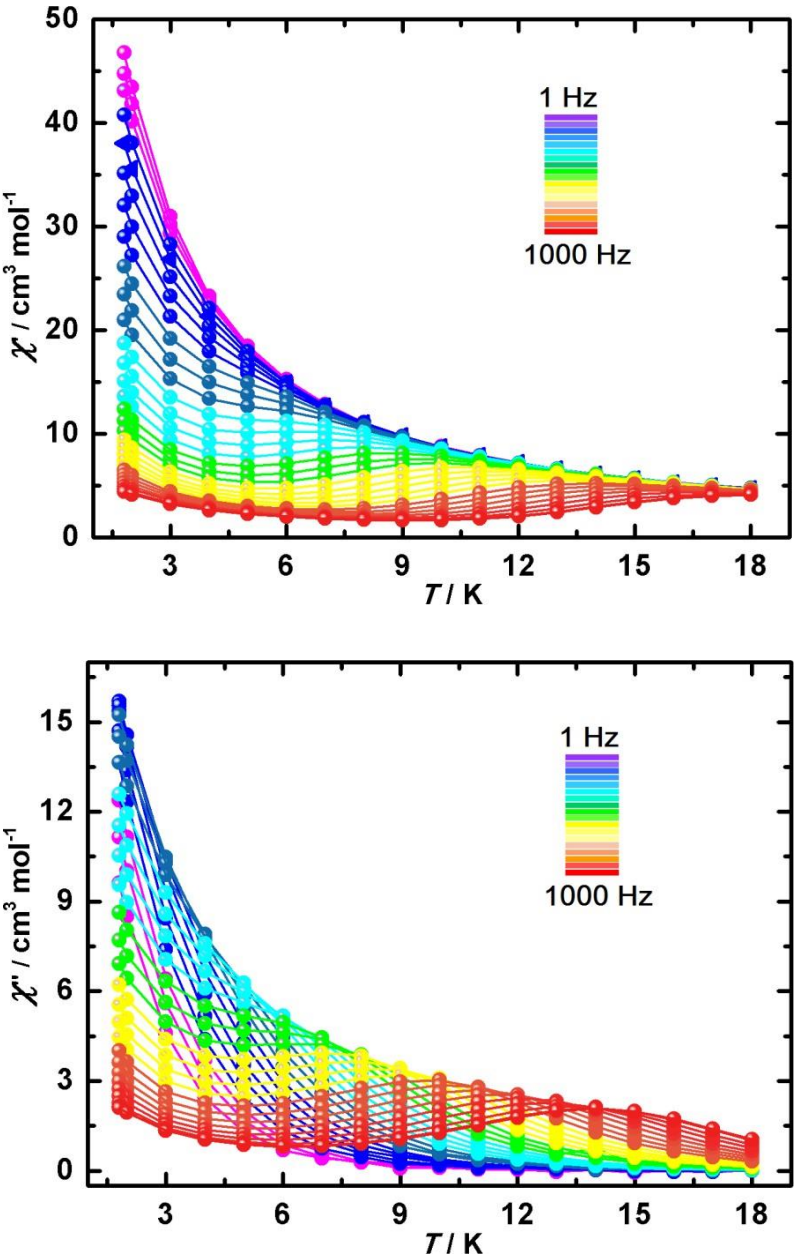

Figure S26. Temperature dependence of the χ' and χ'' of the *ac* susceptibilities under zero-dc field for compound **II**.

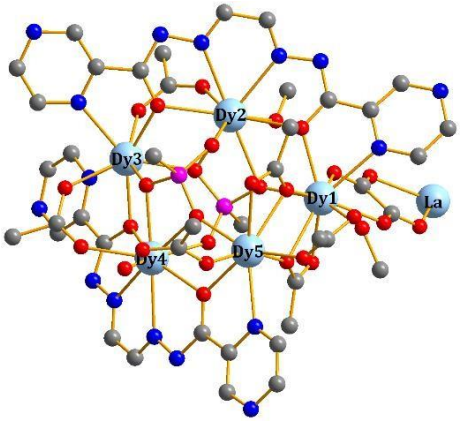

I

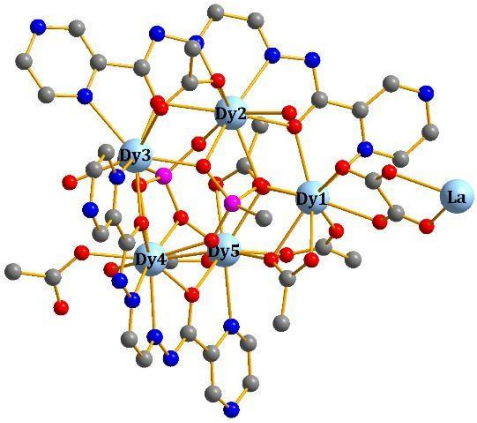

I-UV

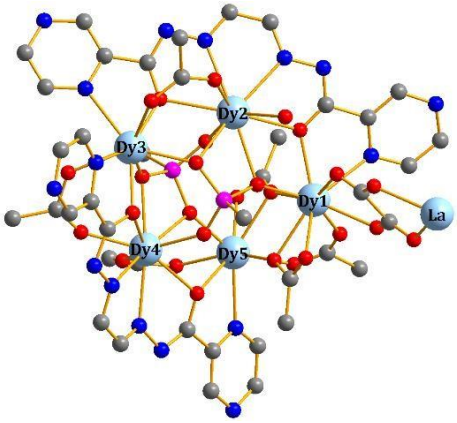

I-A-N_2

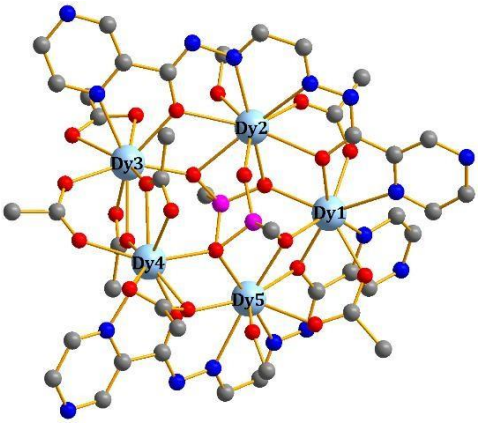

II-molecule A

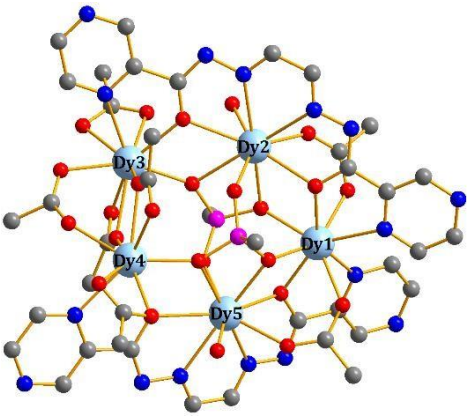

II-molecule B

Figure S27. Calculated model structures of the Dy^{III} fragments of **I**, **I-UV**, **I-A-N_2**, **II-molecule A** and **II-molecule B**. All H atoms are omitted for clarity.

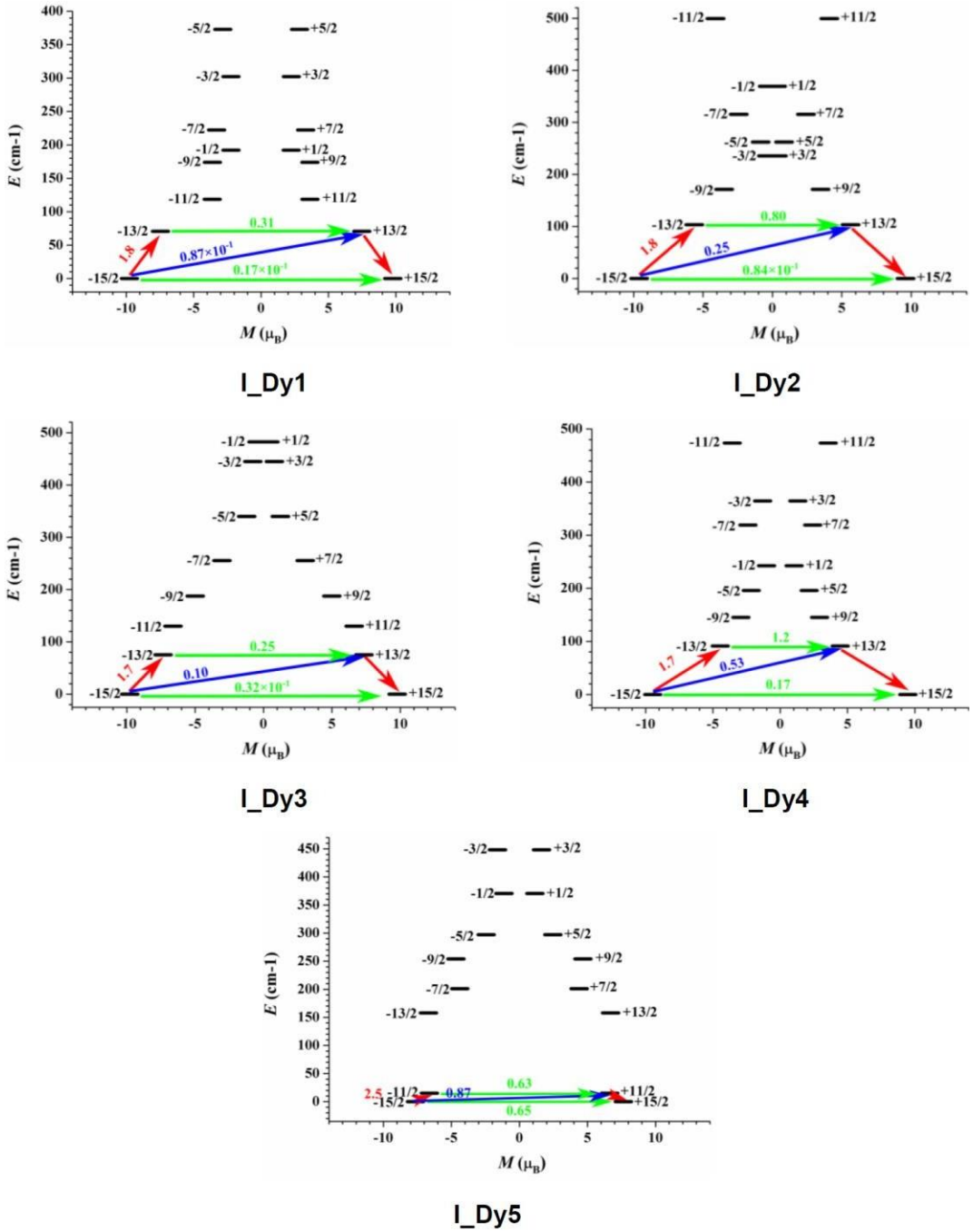

Figure S28. The magnetization blocking barriers for individual Dy^{III} fragments of **I**. The thick black lines represent the Kramers doublets as a function of their magnetic moment along the magnetic axis. The green lines correspond to diagonal quantum tunnelling of magnetization (QTM); the blue line represent off-diagonal relaxation process. The numbers at each arrow stand for the mean absolute value of the corresponding matrix element of transition magnetic moment.

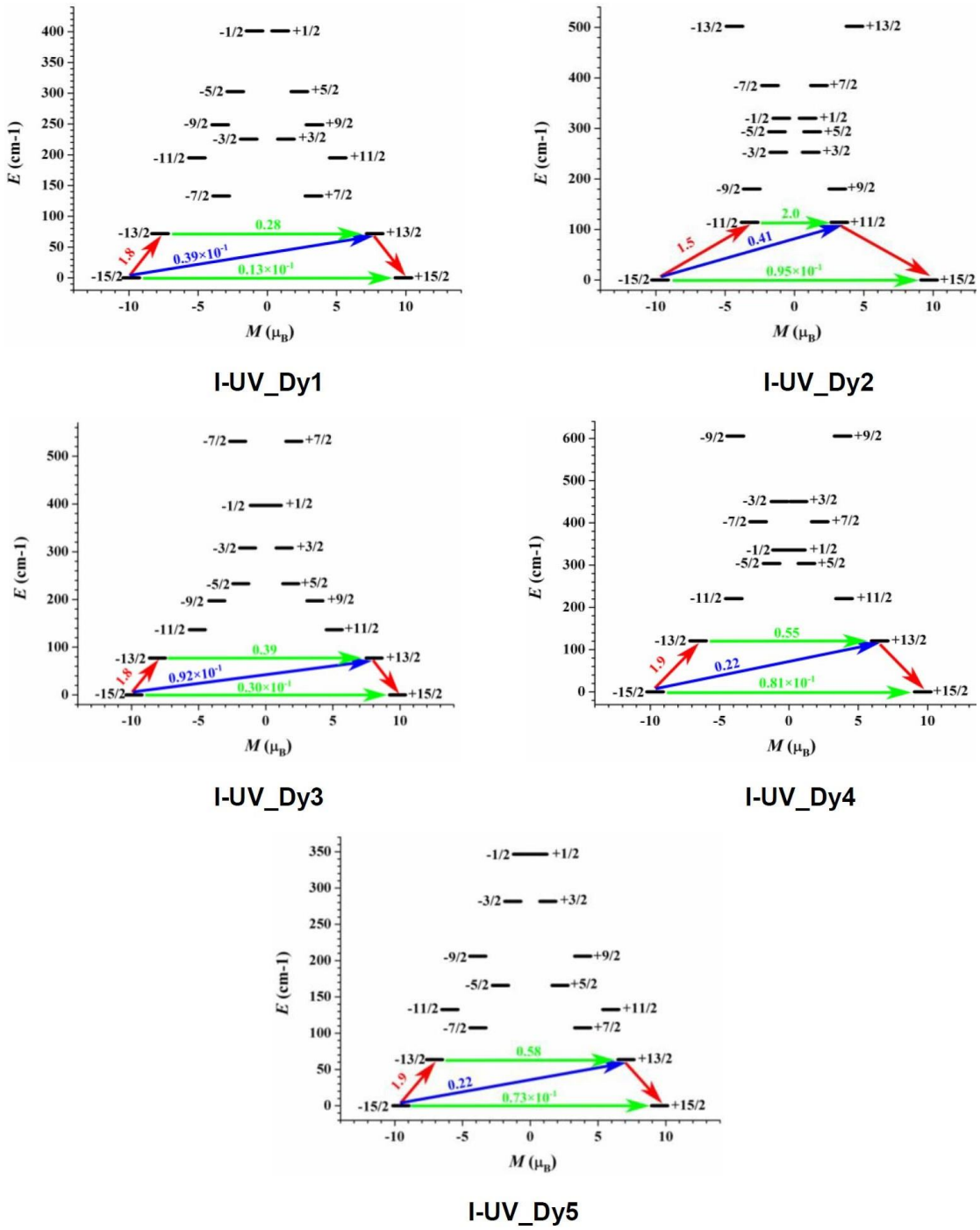

Figure S29. The magnetization blocking barriers for individual Dy^{III} fragments of **I-UV**. The thick black lines represent the Kramers doublets as a function of their magnetic moment along the magnetic axis. The green lines correspond to diagonal quantum tunnelling of magnetization (QTM); the blue line represent off-diagonal relaxation process. The numbers at each arrow stand for the mean absolute value of the corresponding matrix element of transition magnetic moment.

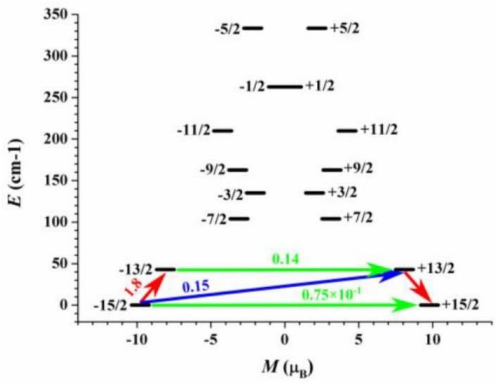

I-A-N$_2$_Dy1

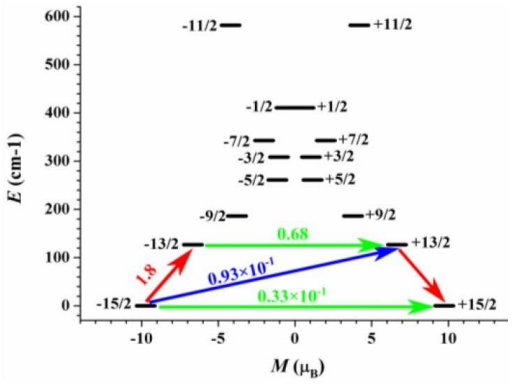

I-A-N$_2$_Dy2

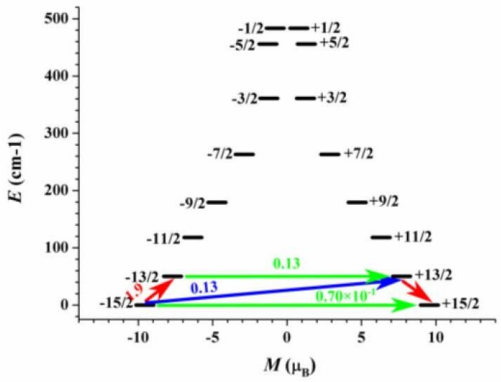

I-A-N$_2$_Dy3

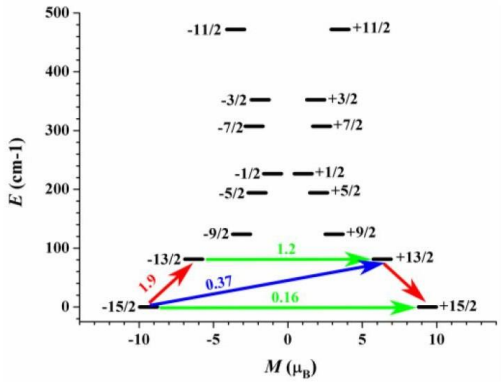

I-A-N$_2$_Dy4

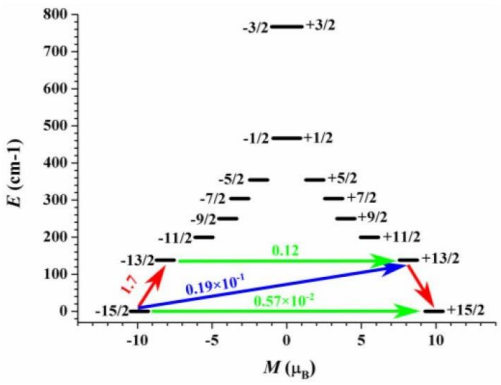

I-A-N$_2$_Dy5

Figure S30. The magnetization blocking barriers for individual Dy^{III} fragments of **I-A-N$_2$**. The thick black lines represent the Kramers doublets as a function of their magnetic moment along the magnetic axis. The green lines correspond to diagonal quantum tunnelling of magnetization (QTM); the blue line represent off-diagonal relaxation process. The numbers at each arrow stand for the mean absolute value of the corresponding matrix element of transition magnetic moment.

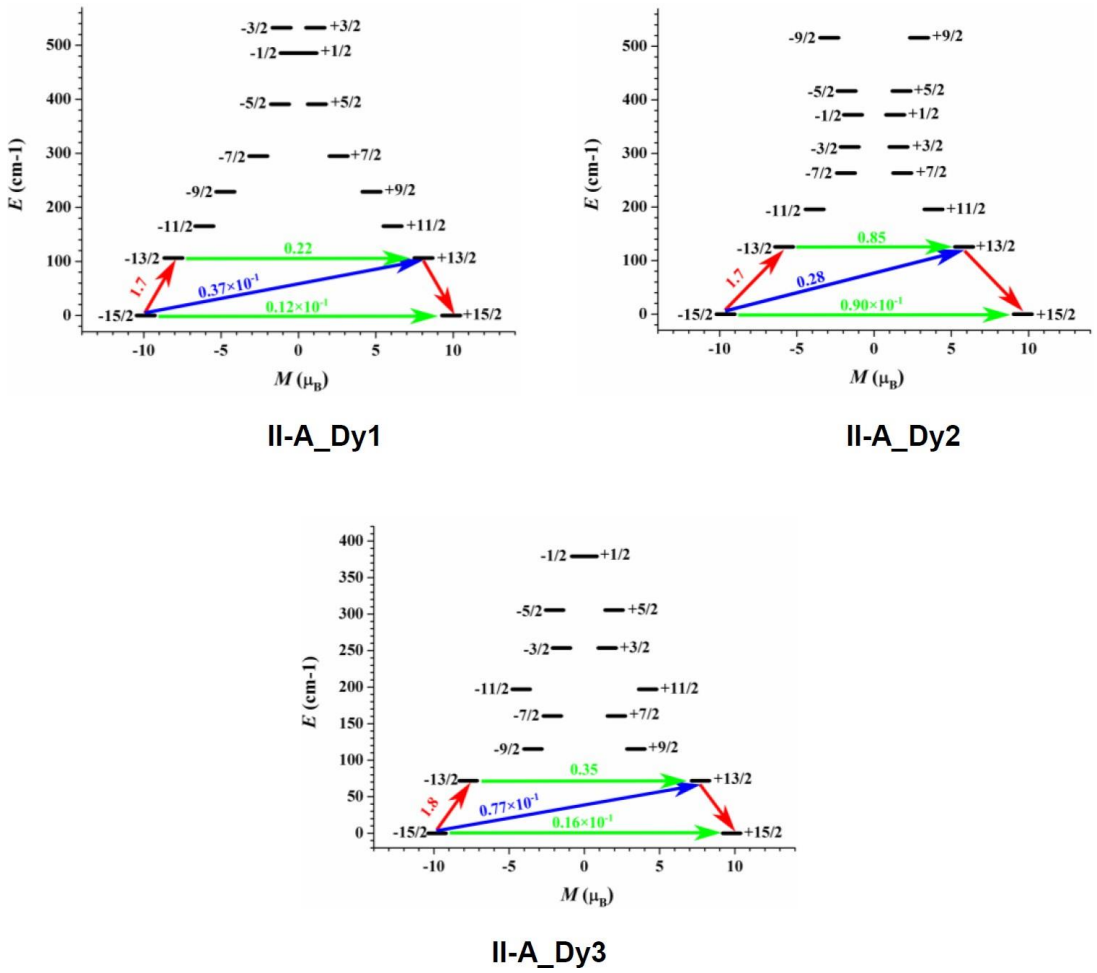

Figure S31. The magnetization blocking barriers for individual Dy^{III} fragments of **II-molecule A**. The thick black lines represent the Kramers doublets as a function of their magnetic moment along the magnetic axis. The green lines correspond to diagonal quantum tunnelling of magnetization (QTM); the blue line represent off-diagonal relaxation process. The numbers at each arrow stand for the mean absolute value of the corresponding matrix element of transition magnetic moment.

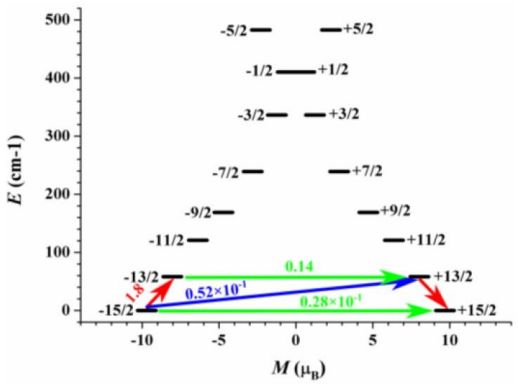

II-B_Dy1

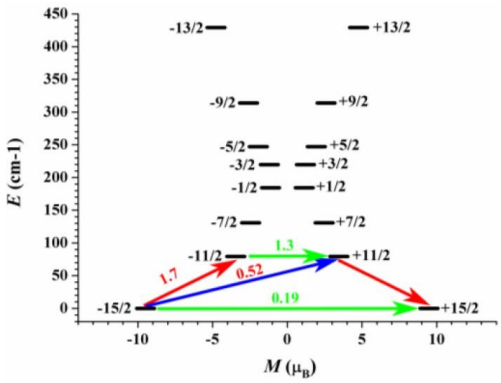

II-B_Dy2

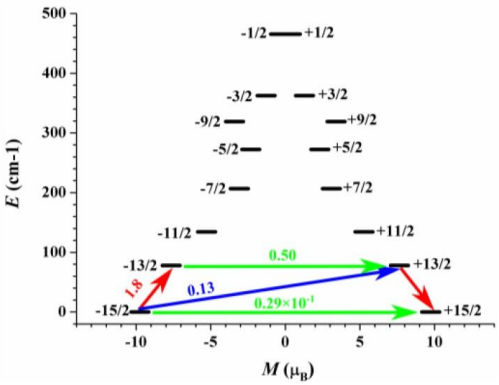

II-B_Dy3

Figure S32. The magnetization blocking barriers for individual Dy^{III} fragments of **II-molecule B**. The thick black lines represent the Kramers doublets as a function of their magnetic moment along the magnetic axis. The green lines correspond to diagonal quantum tunnelling of magnetization (QTM); the blue line represent off-diagonal relaxation process. The numbers at each arrow stand for the mean absolute value of the corresponding matrix element of transition magnetic moment.

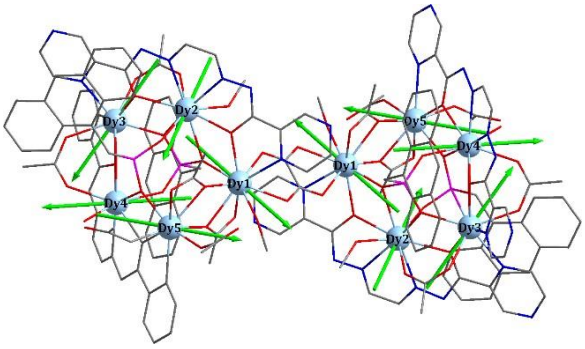

I

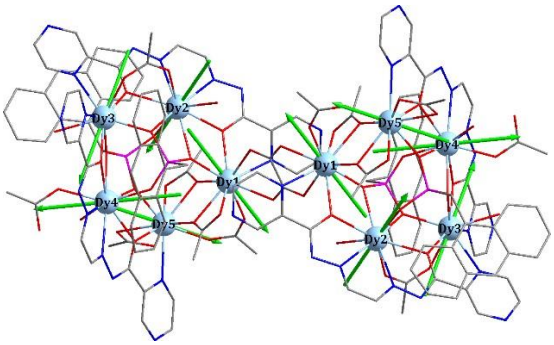

I-UV

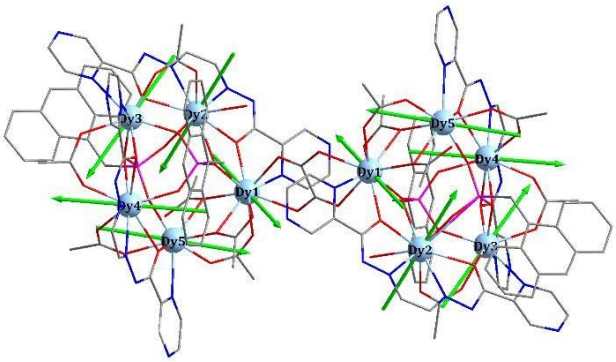

I-A-N_2

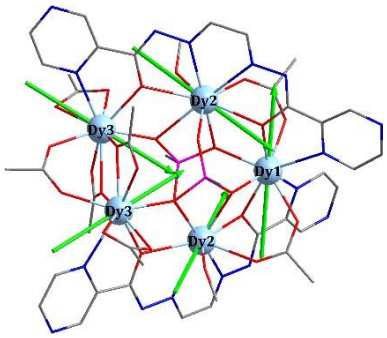

II-molecule A

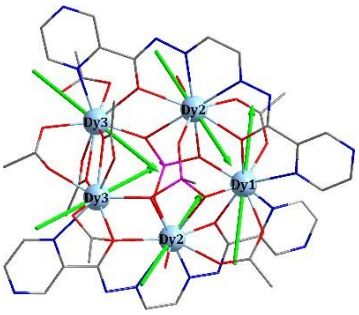

II-molecule B

Figure S33. Calculated orientations of the local main magnetic axes of the ground Kramers doublet on Dy^{III} ions of **I**, **I-UV, I-A-N_2, II-molecule A** and **II-molecule B**.